Copyright Warning & Restrictions

The copyright law of the United States (Title 17, United States Code) governs the making of photocopies or other reproductions of copyrighted material.

Under certain conditions specified in the law, libraries and archives are authorized to furnish a photocopy or other reproduction. One of these specified conditions is that the photocopy or reproduction is not to be "used for any purpose other than private study, scholarship, or research." If a, user makes a request for, or later uses, a photocopy or reproduction for purposes in excess of "fair use" that user may be liable for copyright infringement,

This institution reserves the right to refuse to accept a copying order if, in its judgment, fulfillment of the order would involve violation of copyright law.

Please Note: The author retains the copyright while the New Jersey Institute of Technology reserves the right to distribute this thesis or dissertation

Printing note: If you do not wish to print this page, then select "Pages from: first page # to: last page #" on the print dialog screen

ABSTRACT

MICROFLUIDIC BIOSENSOR WITH FUNCTIONALIZED GOLD NANO PARTICLES ON INTERDIGITATED ELECTRODES

by

Bharath Babu Nunna

The integration of the microfluidics to the biosensor has growing demand with favorable conditions such as reduced processing time and low reagent consumption. The immuno biosensing with the microfluidic platform helped to make the electrochemical biosensing assays portable due to which this sensing mechanism can be easily implemented in point of care devices. The implementation of the biosensing in the microchannels significantly reduces the sample requirement form milli liter (mL) to micro liter (uL), and thus leads to low volume sample requirement during the sensing. The primary factors contributing to the microfluidic biosensors performance are probe immobilization, specific binding and fundamental limits of probe affinity. Due to the tight confinement of the flow of the antigen solution in the microscale, the flows in the microchannel exert high shear stresses on the surface of the microchannel and influence the stability of the immobilized antibodies on the surface. So the study of the sensing signal response during the flow condition attracts many researchers to develop novel techniques of antibody immobilization for enhanced stability.

The study of the sensitivity variation of CA-125 antigens detection using interdigitated electrodes, ‘with’ and ‘without’ microfluidic flow of CA-125

antigens is performed. The CA-125 antibodies are covalently bonded to the interdigitated electrodes using the Thiourea and Glutaraldehyde. When the biofluid sample (CA-125 antigens with phosphate buffer saline solution) is passed on the CA-125 antibodies that are immobilized on the gold interdigitated electrodes, the capacitance variation of the sensing circuit is caused due to the antigen antibody interaction. However, the capacitance measured during CA-125 antigen-antibody interaction with the microfluidic flow condition is lower than ‘without microfluidic flow’ condition due to the instability of the immobilized antibodies on the sensing surface that is caused by the shear stress during the microfluidic flow.

The study of sensitivity variation of CA-125 detection ‘with’ and ‘without’ microfluidic flow of CA-125 antigens is performed using the gold nano particles on the interdigitated electrodes. The carboxylic gold nanoparticles forms covalent bond with the antibodies and the orientational freedom of gold nano particles helps in higher quantity of antibodies immobilized. Though the gold nano particles provide higher stability to the antibodies when compared to the Glutaraldehyde.

The future progress of this research will be detection of multiplex antigens with multiple concentrations in order to enhance the microfluidic biosensing mechanisms to serve in the point-of-care devices in diagnosing targeted disease antigens with high sensitivity.

MICROFLUIDIC BIOSENSOR WITH FUNCTIONALIZED GOLD NANO PARTICLES ON INTERDIGITATED ELECTRODES

by
Bharath Babu Nunna

A Dissertation
Submitted to the Faculty of
New Jersey Institute of Technology
in Partial Fulfillment of the Requirements for the Degree of
Doctor of Philosophy in Mechanical Engineering

Department of Mechanical and Industrial Engineering

May 2018

.

APPROVAL PAGE

MICROFLUIDIC BIOSENSOR WITH FUNCTIONALIZED GOLD NANO PARTICLES ON INTERDIGITATED ELECTRODES

Bharath Babu Nunna

Dr. Eon Soo Lee, Dissertation Advisor — Date
Assistant Professor of Mechanical and Industrial Engineering, NJIT

Dr. Chao Zhu, Committee Member — Date
Professor of Mechanical and Industrial Engineering, NJIT

Dr. Zhiming Ji, Committee Member — Date
Professor of Mechanical and Industrial Engineering, NJIT

Dr. Jacob Trevino, Committee Member — Date
Research Associate Professor of City University of New York

Dr. Dibakar Datta, Committee Member — Date
Assistant Professor of Mechanical and Industrial Engineering, NJIT

BIOGRAPHICAL SKETCH

Author: Bharath Babu Nunna

Degree: Doctor of Philosophy

Date: May, 2018

Education:

- Doctor of Philosophy in Mechanical Engineering,
  New Jersey Institute of Technology, Newark, NJ, USA, 2018
- Master of Science in Mechanical Engineering,
  University of Bridgeport, Bridgeport, CT, USA, 2007
- Bachelor of Technology in Mechanical Engineering,
  Acharya Nagarjuna University, Andhra Pradesh, India, 2004

Major: Mechanical Engineering

Publications, Patents and Presentations:

Journal papers:

B.B. Nunna, D. Mandal, S. Zhuang and E.S. Lee*: Innovative Point-of-Care (POC) Micro Biochip for Early Stage Ovarian Cancer Diagnostics. *Sensors and Transducers.* 214 (7), pp. 12-20 (2017).

D. Mandal, B.B. Nunna (Co-First author), S. Zhuang, S. Rakshit and E.S. Lee*: Carbon Nanotubes Based Biosensor for Detection of Cancer Antigens (CA-125) Under Shear Flow Condition. *Nano-Structures and Nano-Objects.* DOI: 10.1016/j.nanoso.2017.09.013 (2017)

B.B. Nunna, D. Mandal, S. Zhuang and E.S. Lee*: Sensitivity Study of CA-125 Detection Using Interdigitated Electrodes Under Microfluidic Flow Condition. Journal of Micromechanics and Microengineering (2017). JMM-103304 (Under Review)

D. Mandal, B.B. Nunna (Co-First author), S. Zhuang, and E.S. Lee*: Sensitivity Study of Cancer Antigens (CA-125) Using Gold Nano Particles on Interdigitated Electrode – Based Biosensor Under Shear Flow Condition. *Microelectronic Engineering* (2018). MEE-D-18-00194 (Under Review).

S. Zhuang, B.B. Nunna, D. Mandal, E.S. Lee: A Review of Nitrogen-Doped Graphene Catalysts for Proton Exchange Membrane Fuel Cells-Synthesis, Characterization, and Improvement. *Nano-Structures and Nano-Objects* (2017). DOI:10.1016/j.nanoso.2017.09.003

S. Zhuang, B.B. Nunna, J.A. Boscoboinik, and E.S. Lee*: Nitrogen doped graphene catalysts: High energy wet ball milling synthesis and characterizations of functional groups and particle size variation with time and speed. *International Journal of Energy Research*. DOI: 10.1002/er.3821 (2017).

S. Zhuang, E.S. Lee*, L. Lei, B.B. Nunna, L. Kuang and W. Zhang: Synthesis of Nitrogen-Doped Graphene Catalyst by High-Energy Wet Ball Milling for Electrochemical Systems. *International Journal of Energy Research*. DOI: 10.1002/er.3595 (2016).

S. Zhuang, B.B. Nunna, L. Lei, E.S. Lee: New Nitrogen-Doped Graphene/MOF-modified catalyst for Fuel Cell Systems. *ECS Transactions*. 72(8), pp.149-154 (2016).

Conference papers:

B.B. Nunna, D. Mandal, S. Zhuang and E.S. Lee*: A Standalone Micro Biochip to Monitor the Cancer Progression by measuring Cancer Antigens as a Point-of-care (POC) device for enhanced Cancer Management, *IEEE-NIH 2017 Special Topics Conference on Healthcare Innovations and Point-of-Care Technologies*, (PCHT17-0155) Bethesda MD, 6-8 November 2017.

B.B. Nunna, Lee, E.S*. (2017). Point-of-Care (POC) Micro Biochip for Cancer Diagnostics, *TechConnect World Innovation Conference and Expo*, May 14-17, 2017, Washington. D.C.

B.B. Nunna, S. Zhuang, J. Javier, D. Mandal and E.S. Lee* (2016). Biomolecular Detection using Molecularly Imprinted Polymers (MIPs) at Point-of- Care (POC) Micro Biochip, *2016 IEEE-NIH 2016 Healthcare Innovation Point-of-Care Technologies Conference* (HI-POCT16), (PCHT16-0099) November 9-11, 2016, Cancun, Mexico.

S. Zhuang, B.B. Nunna, L. Lei and E.S. Lee*: Synthesis of Nitrogen-doped Graphene Catalyst by Wet Ball Milling for Electrochemical Systems. (Paper ID: 2425505), *251st ACS National Meeting & Exposition*, March 13-17, 2016, San Diego, California.

B.B. Nunna, S. Zhuang, I. Malave and E.S. Lee*. (2015). Ovarian Cancer Diagnosis using Micro Biochip, *NIH-IEEE 2015 Strategic Conference on Healthcare Innovations and Point-of-Care Technologies for Precision Medicine*, (PCHT15-0056) November 9-10, 2015, Bethesda, MD.

Patents:

E.S. Lee, B.B. Nunna, Special Polymer for Biomarker Detection - US PRV Provisional Patent Application No. 62/420,178 filed on Nov 10th, 2016

E.S. Lee, B.B. Nunna, Innovative Nano circuit in Biomarker Detection – US PRV Provisional Patent Application No. 62/420,195 filed on Nov 10th, 2016

E.S. Lee, B.B. Nunna, Self-separation of serum during capillary flow - US PRV Provisional Patent Application No. 62/420,226 filed on Nov 10th, 2016

E.S. Lee, B.B. Nunna, Reduced maintenance air filtration device- US PRV Provisional Patent Application No. 62/421,556 filed on Nov 14th, 2016

E.S. Lee, B.B. Nunna, Enhanced Sensitivity in Biochip for Disease Diagnostics - US PRV Provisional Patent Application No. 62/459,173 filed on Feb 15th, 2017

E.S. Lee, B.B. Nunna, Enhanced Specificity in Biochip for Disease Diagnostics - US PRV Provisional Patent Application No. 62/459,240 filed on Feb 15th, 2017

E.S. Lee, B.B. Nunna, Microfluidic Diagnostic Assembly- US Non-Provisional Patent Application No. PCT/2017/038554 filed on June 21st, 2017

E.S. Lee, B.B. Nunna, A microfluidic biochip with gold nano interdigitated electrodes in the controlled self-driven flow - US PRV Provisional Patent Application No. 62/576,208 filed on Oct 24th, 2017

E.S. Lee, B.B. Nunna, Biosensor with enhanced sensitivity using interdigitated Nano Electrodes and Carbon Nano Tubes. - US PRV Provisional Patent Application No. 62/589,097 filed on Nov 21st, 2017

Conference Presentations:

B.B. Nunna: Point-of- Care (POC) Nano Biochip for Enhanced Cancer Screening. *27th Northeast Regional Conference -NRC 2018*, March 24th 2018, Montclair, NJ.

B.B. Nunna: Innovative low-cost micro biochip for highly accurate disease detection and continuous healthcare monitoring. *2017 Newark Innovation Acceleration Challenge*, 27th Nov 2017, Newark, NJ.

B.B. Nunna, D. Mandal, S. Zhuang and E.S. Lee*: Innovative Point of Care (POC) Nano Biochip for Disease Diagnosis and to Monitor the Disease Progression. *IEEE-NIH 2017 Special Topics Conference on Healthcare Innovations and Point-of-Care Technologies*, (PCHT17-0155) Bethesda MD, 6-8 November 2017.

B.B. Nunna, S. Zhuang and E.S. Lee*: Self-separation of blood plasma from whole blood during the capillary flow in microchannel. (A11.00009) – *70th Annual Meeting of the American Physical Society – Division of Fluid Dynamics Meeting*, 2017, November 19–21, 2017; Denver, Colorado.

B.B. Nunna and E.S. Lee*: Innovative standalone In-Situ Nano Biochip for Instantaneous Disease Diagnostics (Defense Innovation 2017: 2182 & 170). *2017 Defense Innovation Technology Acceleration Challenges*, Oct 3-5, 2017, Tampa, Florida.

B.B. Nunna, S. Zhuang and E.S. Lee*: Point Of Care Micro Biochip For Disease Diagnostics And Continuous Health Monitoring. IPACK2017-74297 & 74298. *ASME InterPACK 2017*. Aug 29th - Sep 1st 2017, San Francisco, CA

B.B. Nunna, S. Zhuang and E.S. Lee*: Self-separation during the self-driven flow of blood in microchannel. (IMECE2017- 72281). *ASME International Mechanical Engineering Congress and Exposition* (IMECE-2016). Nov 3rd - 9th 2017, Tampa, Florida.

B.B. Nunna and E.S. Lee*: Point-of-Care (POC) Micro Biochip for Cancer Diagnostics (Techconnect 2017: 996). *TechConnect World*, May 14-17, 2017, Washington, DC, U.S.A.

B.B. Nunna and E.S. Lee*: Point-of- Care (POC) Micro Biochip for Cancer Diagnostics at – *Dana Knox –NJIT* April 19th, 2017, Newark, NJ

B.B. Nunna: Point-of- Care (POC) Micro Biochip for Cancer Diagnostics at – *NJIT /PCCI fifth Annual Joint Meeting*. March 28th, 2017. Florham Park, NJ.

B.B. Nunna, S. Zhuang and E.S. Lee*: Flow control mechanism of capillary driven flow in microchannel using non-mechanical forces (A25.00002) – *69th Annual Meeting of the American Physical Society – Division of Fluid Dynamics Meeting*, 2016, November 20-22, 2016, Portland, Oregon.

B.B. Nunna, S. Zhuang and E.S. Lee*: Point of Care (POC) Micro Biochip for Ovarian Cancer Diagnostics at Early Stages, (IMECE2016-68853). *ASME International Mechanical Engineering Congress and Exposition* (IMECE-2016). November 11 – 17, 2016, Phoenix, AZ.

B.B. Nunna, S. Zhuang, J. Javier, D. Mandal and E.S. Lee* (2016). Biomolecular Detection using Molecularly Imprinted Polymers (MIPs) at Point-of- Care (POC) Micro Biochip, *2016 IEEE-NIH 2016 Healthcare Innovation Point-of-Care Technologies Conference* (HI-POCT16), (PCHT16-0099) November 9-11, 2016, Cancun, Mexico.

B.B. Nunna and E.S. Lee*: Point-of-Care (POC) Micro Biochip for Ovarian Cancer Diagnostics (Micro Biochip - 798). *National Science Foundation Innovation-Corps NYCRIN workshop*. Aug 28-30, 2016, Newark, NJ

B.B. Nunna, S. Zhuang and E.S. Lee*: Influence on Capillary Flow of Human Blood in PDMS Micro Channels due to various Surface Treatments, (ICNMM2016-8122). *ASME 14th Int'l Conference on Nano- channels, Microchannels and Minichannels (ICNMM)*. July 10–14, 2016, Washington, DC.

B.B. Nunna, S. Zhuang and E.S. Lee*: Point-of-Care (POC) micro biochip for cancer diagnostics (Microfluidic Poster-0002). *2016 Global Engage's Microfluidics Congress: USA.* July 11–12, 2016, Philadelphia, PA

S. Zhuang, B.B. Nunna, L. Lei and E.S. Lee*: Characterization of Nitrogen-doped Graphene Catalyst synthesized by Wet Ball Milling for PEM Fuel Cell (PowerEnergy2016-59376), *ASME Power & Energy Conference*, June 26-30, 2016, Charlotte, North Carolina.

L. Lei, S. Zhuang, B.B. Nunna and E.S. Lee*: Characteristics of Nitrogen doped-Graphene Synthesized Using High Energy Wet Ball Milling (PowerEnergy2016-59480), *ASME 2016 14th Fuel Cell Science, Engineering, and Technology Conference*, June 26-30, 2016, Charlotte, NC.

S. Zhuang, B.B. Nunna, L. Lei and E.S. Lee*: New Non-PGM Catalyst Synthesized By Wet Ball Milling for Fuel Cell Systems, (Abstract # 71275), *229th Electro Chemical Society (ECS) Meeting*, May 29 - June 3, 2016, San Diego, CA.

L. Lei, S. Zhuang, B.B. Nunna and E.S. Lee*: The Characteristics of New Synthesized Metal Organic Framework-Based Catalysts for Fuel Cell Systems (Abstract #71967), *229th Electro Chemical Society (ECS) Meeting*, May 29 - June 3, 2016, San Diego, CA.

B.B. Nunna and E.S. Lee*: Point-of-Care (POC) micro biochip for cancer diagnostics, (2016–CFN04). *2016 NSLS-II & CFN Joint Users' Meeting at Brookhaven National Laboratory*. May 23–25, 2016, Upton, NY.

B.B. Nunna and E.S. Lee*: Point-of-Care (POC) Micro Biochip for Ovarian Cancer Diagnostics, *2016 Dana Knox Student Research Showcase at NJIT*. April 20, 2016, Newark, NJ

B.B. Nunna and E.S. Lee*: Point-of-Care (POC) Micro Biochip for Ovarian Cancer Diagnostics, *4th Annual NJIT Innovation Day 2016 at NJIT*. April 15, 2016, Newark, NJ

B.B. Nunna and E.S. Lee*: Point-of-Care (POC) Micro Biochip for Ovarian Cancer Diagnostics, *New Jersey Entrepreneurial Network (NJEN) 2016* - Posters, Pitches and Prizes at Princeton. (March 1, 2016), Princeton, NJ

B.B. Nunna, S. Zhuang and E.S. Lee*: Squeeze Flow With Capillary Effect In Nano Imprint Lithography (NIL) Process (M1.00004) – *68th Annual Meeting of the American Physical Society – Division of Fluid Dynamics Meeting*, 2015, November 22-24, 2015, Boston, MA

B.B. Nunna, S. Zhuang and E.S. Lee*: Hemorheology In PDMS Micro Channel With Varied Surface Roughness (KP1.00116) – *68th Annual Meeting of the American Physical Society – Division of Fluid Dynamics Meeting*, 2015, November 22-24, 2015, Boston, MA

B.B. Nunna, S. Zhuang, I. Malave and E.S. Lee*. (2015). Ovarian Cancer Diagnosis using Micro Biochip, *NIH-IEEE 2015 Strategic Conference on Healthcare Innovations and Point-of-Care Technologies for Precision Medicine*, (PCHT15-0056) November 9-10, 2015, Bethesda, MD.

B.B. Nunna, S. Zhuang and E.S. Lee*: Hemorheology in PDMS micro channel, (AJK2015-140676). *ASME-JSME-KSME Joint Fluids Engineering Conference*. (July 26- 31, 2015), Seoul, Korea.

Awards and Honors

'Winner of NIAC- 9th Newark Innovation Acceleration Challenge'- with fellowship of $3000 from Capital One- by Greater Newark Enterprise Corporation and New Jersey Innovation Acceleration Center, Nov 27th, 2017, Newark, NJ

'Best HI-POCT Design Award' at IEEE-NIH 2017 Healthcare Innovations and Point-of-Care Technologies -HI-POCT, (PCHT17-0021) November 6-8, 2017, Bethesda MD.

'2017 Defense Innovation Award' for the submission No: 2182 at 2017 Defense Innovation Summit (DITAC), Oct 23-25, 2017, Tampa, Florida.

'2017 National Innovation Award' for the submission No: 2133 at 19th TechConnect World Innovation Conference & Expo, May 14 -17, 2017, Washington, DC.

'National Science Foundation Travel Support Award' (CMMI- 1649149) to American Society of Mechanical Engineers: International Mechanical Engineering Congress and Exposition conference (ASME-IMECE 2016 & 2017)

'Scientist-in-Residence: 2016' – New York Academy of Sciences and New York Department of Education.

'National level NSF Innovation-Corps Award' -2016 (IIP-1643861) Sponsored by National Science Foundation, Federal, $ 50000. E.S. Lee, (Principal Investigator), B.B. Nunna (Entrepreneurial Lead) and M. A. Ehrlich (Entrepreneurial Mentor).

I would like to dedicate this dissertation to my wife 'Saru',

for all her love and support.

ACKNOWLEDGMENT

Immeasurable appreciation and deepest gratitude for the help and support are extended to the following persons who in one way or another have contributed in making this dissertation possible.

Prof. Eon Soo Lee, my PhD advisor. Thanks for his strong support to my dissertation experiments and his valuable comments and suggestions that helped me in the successful completion of this dissertation. His encouragement and concern has helped me to overcome the difficulties and hardships in the research.

I would like to thank my gracious parents, Sri. Siva Rama Krishna Nunna and Smt. Satyavathi Nunna for all the love, support and encouragement throughout my life.

I also appreciate my peers Shiqiang Zhuang and Debdyuti Mandal in the Advanced Energy Systems and Microdevices Laboratory. Thanks for their support and encouragement during the period of doing this dissertation.

I acknowledge the financial support from Advanced Energy Systems and Microdevices Laboratory, New Jersey Institute of Technology (NJIT) research grant, as well as the technological support from the Center for Functional Nanomaterials at Brookhaven National Laboratory. Finally, thanks for the administrative support from the department of Mechanical Engineering and Industrial Engineering at NJIT.

TABLE OF CONTENTS

TABLE OF CONTENTS

(Continued)

TABLE OF CONTENTS

(Continued)

Chapter **Page**

LIST OF FIGURES

LIST OF FIGURES
(Continued)

LIST OF FIGURES
(Continued)

CHAPTER 1

INTRODUCTION

The concept of biosensing is primarily defined as a recognition element of the biomolecule to confer the selectivity and a transduction element of signal to perform quantitative analysis [1-3]. The nature of the biomolecule interaction with the analyte molecules defines the classification of the recognition element. In the affinity-based, biosensor the immobilized capture probe (such as antibody) that binds the molecule being sensed or targeted in the analyte, and thus detect a change at a localized surface. A better sensing component is designed and developed in such a way so that its interaction with specific analyte produces an effective measurable signal. Biosensors based on transducer components can be classified majorly into Optical, Electrochemical and Piezoelectrical types of biosensor [58-62]. Optical sensors techniques faces great challenges in term of developing simple, portable and inexpensive setups and models. The optical method requires periodic rinsing to prevent biofouling and also, optical sensors are limited in laboratory because the detection instrumentation is too bulky, sophisticated, lacking portability for point-of-care use. In optical biosensors, the biological sensitive element is immobilized onto the surface of the transducer and the biological interaction is withered by generating an optical signal, such as fluorescence or by undergoing changes in optical properties such as adsorption, reflectivity, emission and refractive index. The different techniques for optical based biosensors are Interferometry,

Total internal reflection fluorescence, Surface Plasmon Resonance and Surface enhanced Raman scattering. These mechanisms require very sophisticated and massive setup. The desire of our research is to have higher sensitivity within a small space and setup. The Piezoelectric based is another mass based biosensor which suffers sensitivity problems. Piezoelectric based biosensors consist of flexible mass sensitive structures where one of their surfaces is functionalized with probe molecules. The biological interaction with the appropriate target analytes induces surface stress variations that results in the deflection of the structure. The setup is very complex and challenging to construct. In most cases, cantilever bending is detected by optical methods which again suffer the problems similar of an optical biosensor.

Another bigger challenge faced by piezoelectric method is that the measurements are difficult in opaque medium such as blood. Piezoelectric detection is comparatively less sensitive and temperature dependent that is a major drawback. The mass based biosensors are complex and complexity varies as per the interaction [58-62]. Micro machined ultrasonic transducer is mass sensitive based device in which the surface membrane is covered with sensitive layer and during the interaction with the appropriate analyte the element mass increases and the changes in frequencies are observed. These devices serve well in the chemical sensing applications but biological sensing is not yet reported promising [59]. Therefore, there is need for the development of a portable, inexpensive and in-vitro

electrochemical based biosensor for on-site sample screening. The electrochemical technique is rapidly developing as this technique encounters all the challenges faced by other sensing methodologies. Therefore, there is need for the development of a portable, inexpensive and in-vitro electrochemical based biosensor for on-site sample screening.

The electrochemical biosensors are analytical devices that are fabricated by modifying the surfaces of the electrodes with the biomolecules [55-57]. The principles of electrochemistry are employed to generate the measurable electrical signal during the antigen-antibody interaction in the electrochemical immuno-biosensing [5 & 6]. . The electrochemical technique enables to directly provide information on the event of biorecognition that includes induced capacitance and resistance changes at the electrode or the substrate surfaces allowing for label-free biosensing. The immuno-biosensing is based on the affinity that relies on the binding of the specific antigen to the specific antibody [4]. The electrical immuno-biosensors are classified into voltametric, amperometric, impedance or capacitive sensors based on the measured electrical signal during the biomolecule interaction. [7 & 8]. Voltammetry and amperometry involve measuring the current at an electrode as a function of the applied electrode-solution voltage; these approaches are applied using DC or pseudo-DC and intentionally change the electrode conditions. In contrast, capacitive biosensors measure the electrical capacitance of an interface in AC steady state with constant DC bias conditions. As

discussed below, most often this is accomplished by imposing a small sinusoidal voltage at a particular frequency and measuring the resulting current. The measurement of capacitance is performed at different frequencies to identify the signal responses corresponding to the changes on the electrode surface [63].

Interdigitated electrode-based impedance biosensor is used due to its label-free operation, ease of miniaturization and low cost. The interdigitated electrodes based electrochemical sensing techniques have drawn greater attention in recent years due to their high sensitivity within a smaller setup. Zhu et.al reported the enhancement of the sensitivity by 100 times using interdigitated nano biosensor compared to conventional biosensor for detection of reversible redox species [64]. The interdigitated electrodes based biosensor has advantages like miniaturized size, mass production, low power consumption and ease to operate [65]. The interdigitated electrodes based biosensor produces a capacitive signal which is used as the detection principle [66-68]. The biomarkers possess electrical charge distribution which produces unique signal under the electrical field generated by the interdigitated electrodes [66]. The biomarker interaction or the conjugation produces interference in the electric field which changes the dielectric values of the medium that gives certain capacitance values which is measured and analyzed [69-70].

For enhanced binding capabilities of the biomolecules on the sensing platform, the nanoparticles and the nanotechnology have attracted attention in recent years for their potential applications [15-19]. The nanoparticles with unique

surface chemistry & electrical properties, and also being in the size that is in the range of the biomolecules make them favorable for the biosensing. The nanoparticles are biocompatible which enables it to attach various functional groups like proteins, ligands, peptides, DNA, fatty acids and plasmids for serving the sensing purpose [71-72]. There are various noble metals like gold, silver, palladium, rhodium, platinum etc. which are biocompatible [73]. Although there are various noble metals which can serve the purpose for biosensing, the gold nanoparticles are found to be promising and better for biosensing due to its unique surface chemistry, high electron densities, chemical inertness and it possesses both good electrical and optical properties [74]. The gold nanoparticles help in improving the sensitivity and actively targets the biomarker as it provides the platform for high surface to volume ratio [75-76].

The integration of the microfluidics to the electrical immuno biosensing has growing demand with favorable conditions such as reduced processing time and low reagent consumption [10]. The immuno biosensing on the microfluidic platform helped to make the electrochemical biosensing assays portable due to which this sensing mechanism can be easily implemented in point of care devices [11]. The implementation of the biosensing in the microchannels significantly reduce the sample requirement form milli liter (mL) to micro liter (uL) or pico liter (pL), which helps the detection process especially when the samples like blood are highly precious. However the microfluidic flow of the fluid, due to its dynamic condition

cause some instability on the sensing mechanism [12-14]. The primary factors contributing to the microfluidic biosensors performance are probe immobilization, specific binding and fundamental limits of probe affinity. Due to the tight confinement of the flow of the antigen solution in the microscale, the flows in the microchannel exerts high shear stresses on the surface of the microchannel and influence the stability of the immobilized antibodies on the surface [77-78]. So the study of the sensing signal response during the flow condition attracted many researchers to develop novel techniques of antibody immobilization for enhanced stability. Daniels, Jonathan S et al has reported that the microfluidic biosensor performance can be enhanced with further research on the probe immobilization techniques [79]. An improved understanding of the relation between the antibody binding and the capacitance change would enable the improved biosensor design and the sensitivity. Though there are multiple recent studies performed by researchers such as Goddard and Erickson et al and has studied the stability of the biomolecules under the shear flow condition, most of them are limited to the study DNA immobilization and pressure driven flows [30-80].

This research is primarily intended to understand the capacitance variation of interdigitated based microfluidic biosensor under the microfluidic flow condition. The study is performed on sensing signal response of Cancer Antigen (CA-125) when the CA-125 antibodies are immobilized on the surface of the interdigitated electrode circuit of the capacitive biosensor. The primary study is performed on the

sensitivity variation when the antibodies are immobilized on the sensing platform without nano particles, instead used the chemical treatment for immobilization. The electrode surface was treated with Thiourea and Glutaraldehyde to immobilize the antibodies to the surface of the electrodes. In the next study the the sensitivity variation when the antibodies are immobilized on the sensing platform with carboxylic gold nano particles. The experimental details and the results generated are discussed in detail in chapters 3 and 4.

CHAPTER 2

FABRICATION OF THE BIOCHIP

2.1 Design of the Biochip with Interdigitated Electrodes in the Microchannel

The microfluidic biochip incorporates straight hydrophilic microchannels (515 um width and 107um height) to have the biofluid sample flow without any need of external devices and capacitance sensing mechanism with nano interdigitated electrodes on the surface of the microchannels as shown in Figure 2.1

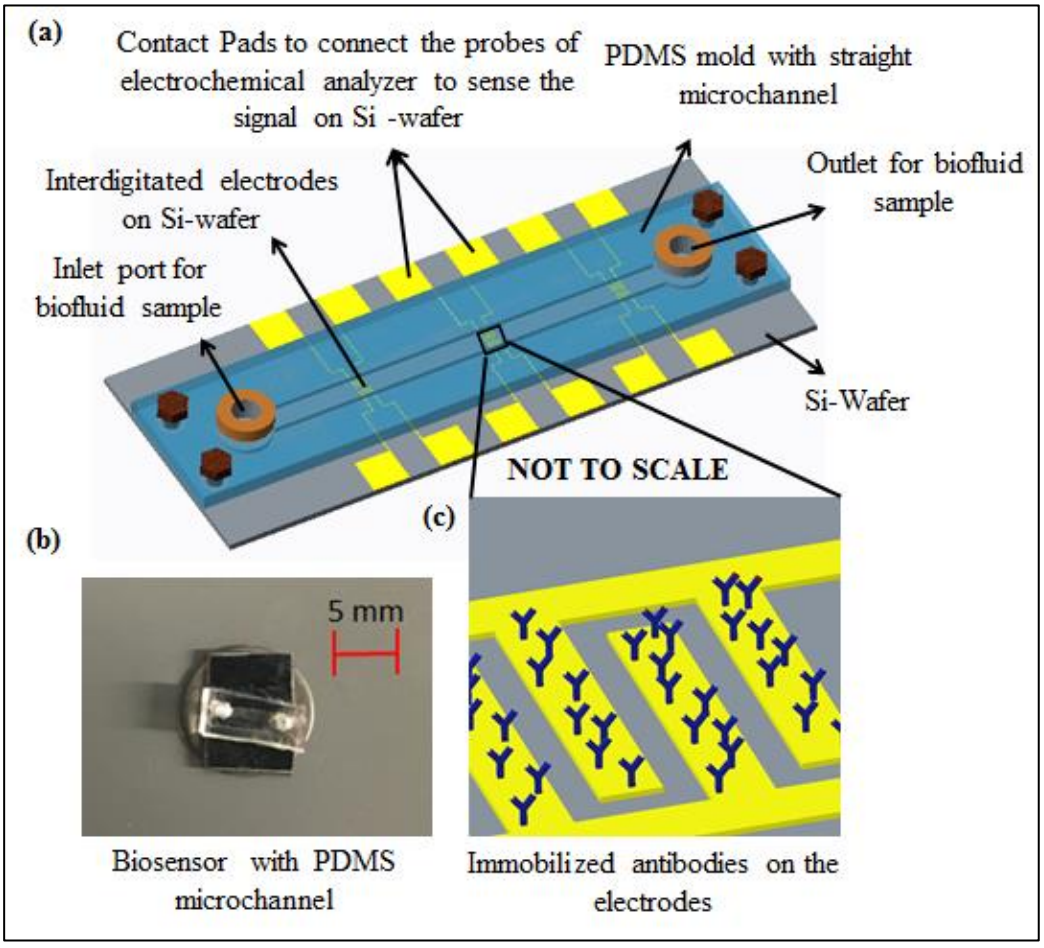

Figure 2.1 (a) The schematic of microfluidic flow setup on the sensing surface (b) The image of the biosensor with the microfluidic setup that is used for these experiments (c) The schematic of the immobilized antibodies on the interdigitated electrodes.

The biofluid sample with the cancer antigens flow in the microchannel interacts with the cancer antibodies that are immobilized on the surface of the interdigitated electrodes. These interactions of the antigen and antibody change the electrical signal of the circuit as shown in Figure 2.2.

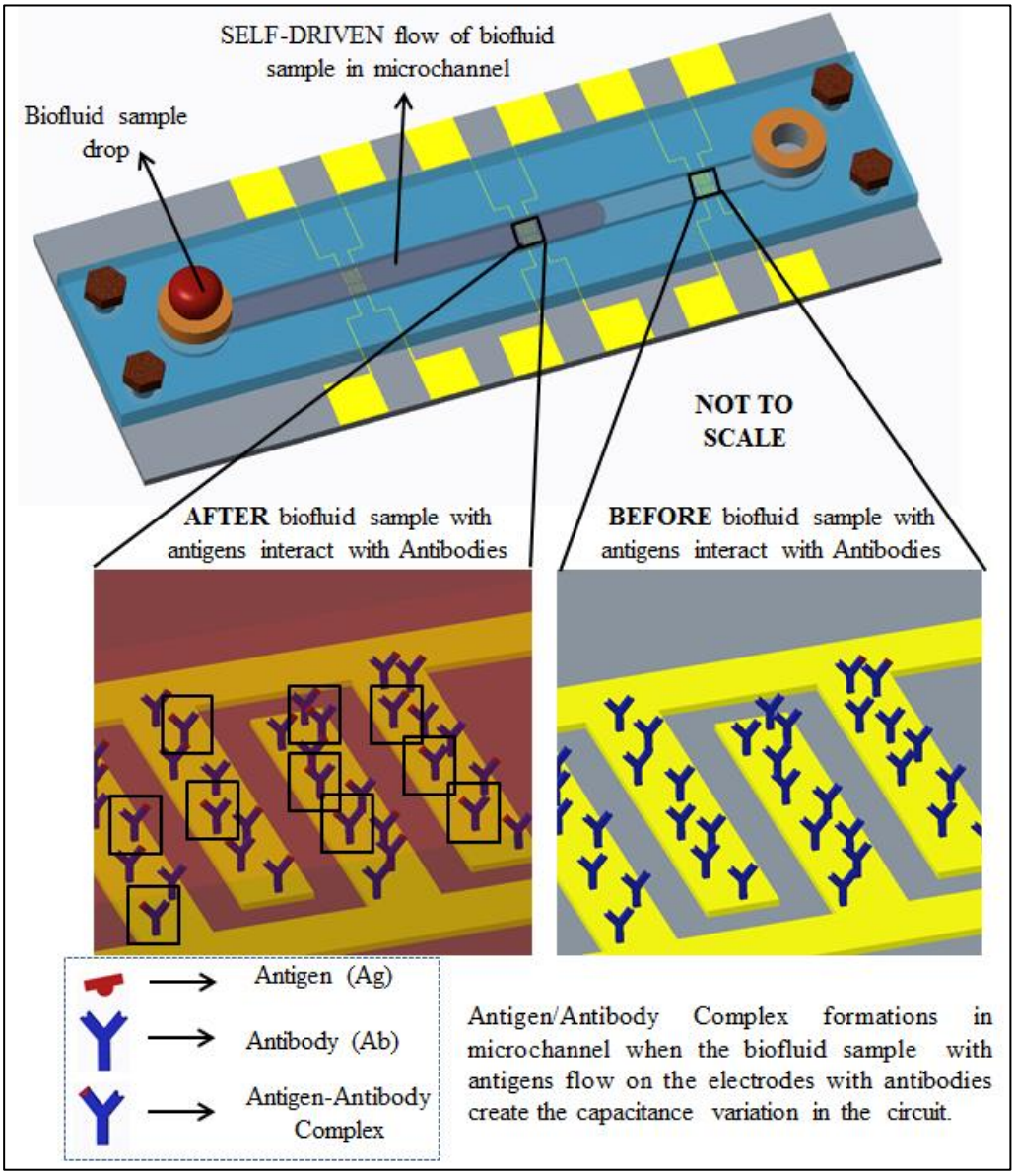

Figure 2.2 The schematic illustration of (a) microfluidic flow of the biofluid in the microchannel (b) 'After' the antigen-antibody interaction (c) 'Before' the antigen-antibody interaction.

In the biochip, an electrical methodology (measuring the change in capacitance)

is implemented for the sensing antigen-antibody interaction. The fabrication of the biochip is primarily incorporated with 2 steps:

1. Fabrication of the hydrophilic PDMS microchannel
2. Fabrication of the sensing platform with interdigitated electrodes for capacitance measurement.

2.2 Fabrication of the Hydrophilic PDMS Microchannel

The biochip incorporates microchannels in order to serve two primary criteria:

- To control the self-driven flow of biofluid sample in the microchannel with no external flow control devices.
- To enhance the interaction between biofluid and the sensing mechanism with high surface area to volume ratio.

Minimizing the external device requirement for flow generation in the microchannel helps to reduce high sample volume (from milliliter to microliter) requirements and reduces the contamination of the biofluid sample. When the blood drop comes in contact with the micro capillary channel, the surface tension of the blood draws the drop into the microchannel and induces the fluid into motion. The capillary flow is generated due to the natural characteristics of the surface of the microchannel and its interaction with the fluid. Capillary action is the result of both adhesion force (between the fluid and the walls of channel) and surface tension of the fluid. Surface tension is the tensile force attained by the interface due to the imbalance of the cohesive forces of the molecules on the interface and the inner molecules of the fluid. The adhesion force (attraction force between the solid and liquid molecules) of

blood with the surface of the microchannel causes the forward force at the edges. The surface tension will hold the surface intact and induce the whole liquid surface to move forward instead of moving only at the edges. The surface tension quantifies the capillary phenomena.

The primary steps involved in the fabrication of hydrophilic PDMS microchannel are:

- Fabrication of Silicon Wafer with microchannels
- Fabrication of PDMS mold with microchannels
- Surface treatment of PDMS (hydrophobic to hydrophilic)

2.2.1 Fabrication of Si-wafer with Microchannels

The Silicon wafers with microchannels are fabricated at the Center for Functional Nano materials at Brookhaven National Laboratory, Upton, New York. A silicon wafer of 4 inch diameter and 1mm thickness is used to fabricate the microchannels on it (An ample Si- wafer thickness (1mm) is chosen, since the channel structures are etched from Si wafer which are 100um to 200um height).

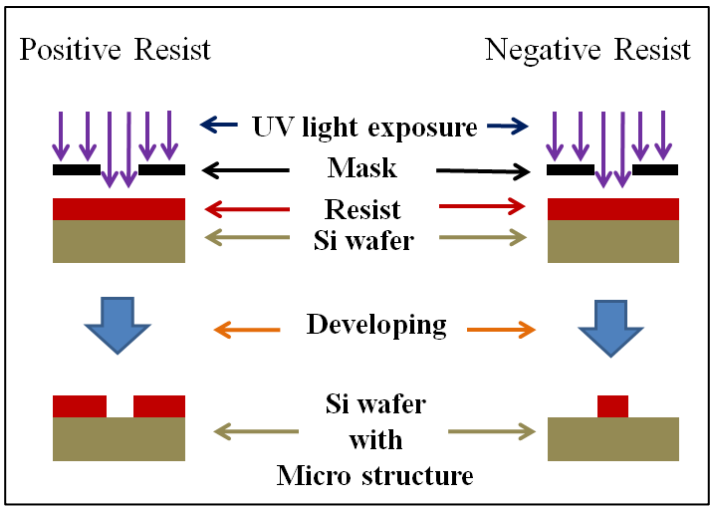

Figure 2.3 Schematic representation of photolithography process for both positive and negative resist on Si wafer.

In the current fabrication method, a positive photo resist is used so that the areas that are chromed are left open as shown in Figure 2.3. The photoresist areas exposed to the UV rays will become soft and removed when developed with the developer. A quartz glass with the micro channels are chromed with the microchannels of various sizes (200um, 300um, 500um and 1000um width) of different shapes like straight channel, serpentine channel, round edged serpentine channel and spiral channel.

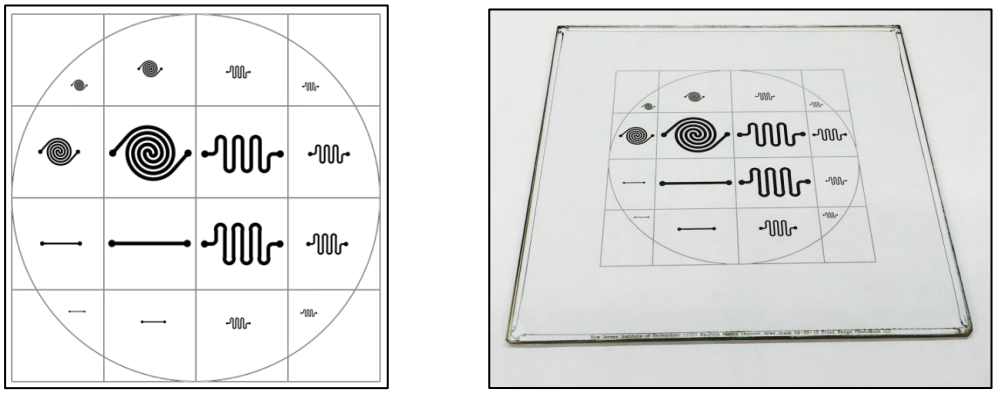

Figure 2.4 The 2d drawing of micro channel structures (Left) & quartz glass with micro channels chromed (Right).

The micro channels of various sizes and shapes are designed and aligned to arrange on a 4 inch wafer as shown in Figure 2.4. The channel structures are chromed on the quartz glass as the positive photo resist is being used in the photo lithography process.

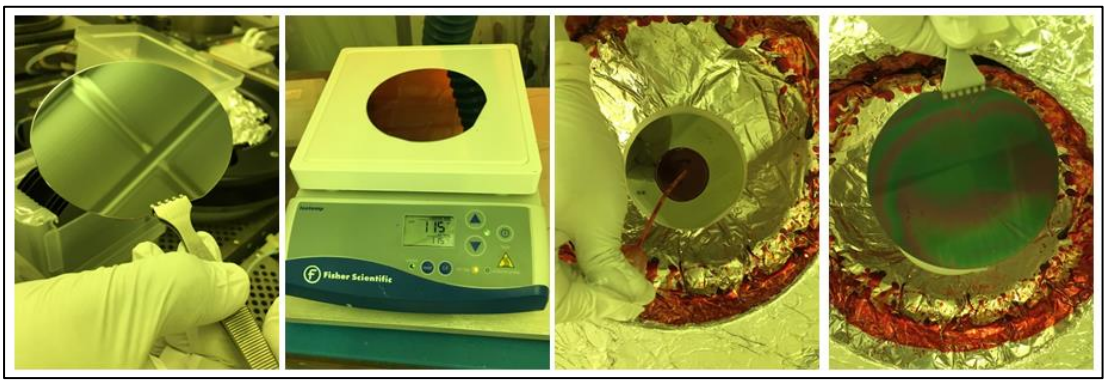

Figure 2.5 Silicon wafer for photo lithography process, Silicon wafer on hot plate, Spin coating the photoresist on Si wafer & Si wafer with photoresist (left to right).

Figure 2.6 Si wafer with photoresist on hot plate, Karl Suss MABA6 mask aligner for UV exposure, developing the Si wafer with CD-26 & Drying Si wafer with nitrogen gun (left to right).

A Silicon Wafer of 4-inch diameter is cleaned with acetone, Isopropanol alcohol and DI water. The wafer is dehydrated at 115°C for about a minute using a hot plate and kept on a cold plate to attain room temperature. A positive photoresist (SPRTM 955) is deposited on top of the wafer. The Si wafer, which is coated with photoresist is placed on a spin coater using a specific size chuck and the spin coater is rotated at 1200 rpm for one minute, which removes the excess photoresist, leaving a thin layer of (micro meters) of SPRTM 955 on the wafer. Coated Si -wafer is placed on the UV light exposure tool (Karl Suss MABA6) with exposure time as 14 seconds. Due to UV exposure, the area which is not covered by mask becomes soft. The wafer needs to be treated with CD-26 chemical and DI water to remove the photoresist remaining on the wafer on the UV exposed area. Wafer is then dried with a nitrogen gun to remove any water content as shown in Figure 2.5 and 2.6

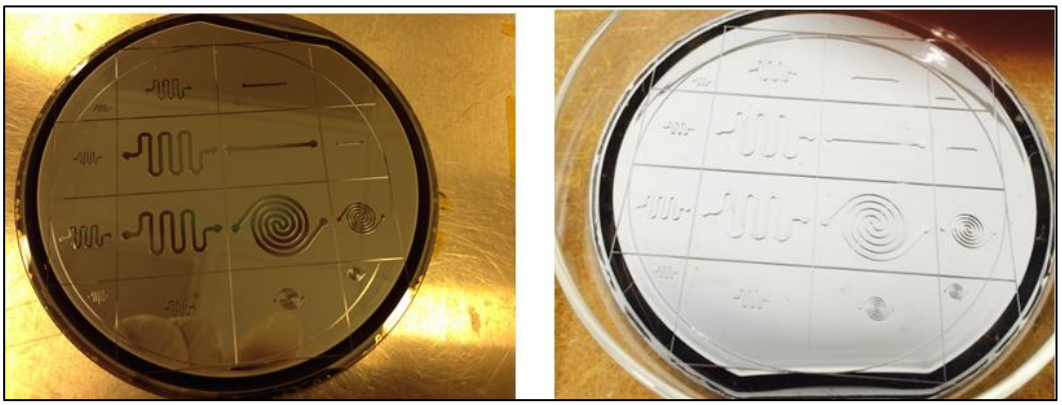

Figure 2.7 Si wafer after the photolithography process (channels formed from photo resist)-Left & Si wafer after the dry etching process with micro channels of height 107um- Right.

A Deep Reactive Ion Etching (DRIE), also called the Bosch process is performed to etch more depth (107um). Areas not covered by the photoresist are etched from the Si wafer, so that the channels are formed. The height of the channels attained is 107um as shown in Figure 2.7.

2.2.2 Fabrication of the PDMS Mold with Microchannels

The PDMS (polydimethylsiloxane) is used to form the mold with the microchannels as cavities. These cavities when covered with the silicon wafer forms the closed microchannel. Figure 2.8 is the schematic of the various steps in the fabrication of the PDMS mold with micro channels.

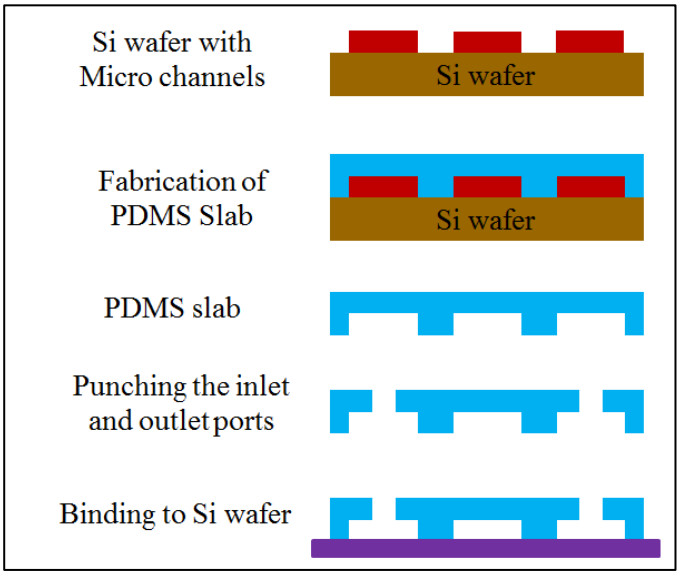

Figure 2.8 Schematic of the PDMS molds fabrication process using Si wafer with micro channel structures.

PDMS Base is blended with a curing agent in definite proportion (1:10). Thorough mixing (about 10 minutes of whisking) is needed to make sure that the curing agent is uniformly distributed. This will ensure that the final PDMS mold is uniformly cross linked between base and curing agent. Degassing is performed multiple times so that all the air bubbles trapped in the PDMS mixture are removed. Curing of the PDMS primarily depends on temperature and time. The curing temperature is indirectly proportional to the time.

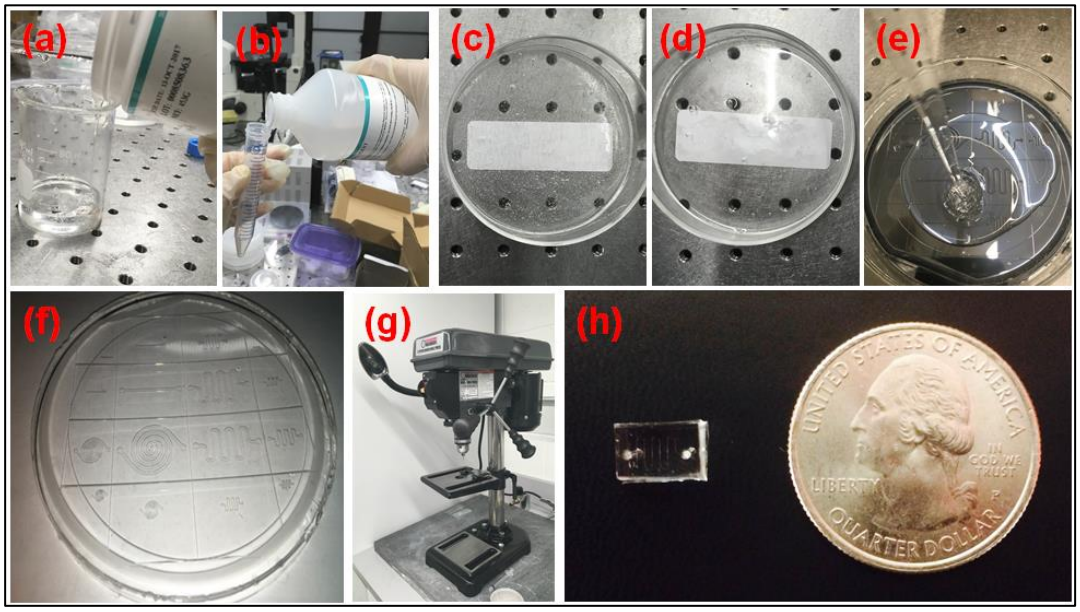

Figure 2.9 (a) The PDMs base (b) PDMS curing agent (c) mixtire of PDMS base and curing agent with air bubbles (d) PDMS mixture after treated with vacuum to remove all the air bubbles (e) PDMS mixture on the Si mold with microchannels (f) PDMS mold with microchannels (g) micro hole punching machine (h) PDMS mold with straight channel of 200um width beside US quarter coin for size comparison.

The PDMS is cured at 100°C for 35 minutes. When PDMS is suitably cured, application of a steady pressure should help peel off the PDMS from Si wafer mold. Though PDMS is a soft material, punching a hole at the inlet and outlet of the microchannel is a critical process due to the micro dimensions. The micro hole punching machine (Central Machinery, 5-Speed bench drill press) is used to make holes in the PDMS mold. These holes act as inlet and outlet for the microchannel as shown in Figure 2.9.

2.2.3 Surface Treatment of PDMS (Hydrophobic to Hydrophilic)

The PDMS (polydimethylsiloxane) is hydrophobic surface (whose contact angle is greater than 90 degrees) by nature, which resists the wettability of fluid on the surface. For the liquid to flow naturally, a hydrophilic surface (whose contact angle is less than

90 degrees) is required. The hydrophobic nature of the PDMS can be altered to a hydrophilic nature by performing various surface treatments like active group attachments [24], Oxygen plasma treatment [25] chemical coating [26], and thermal aging [27]. Oxygen plasma treatment was used to convert hydrophobic nature of PDMS to hydrophilic nature. The hydrophilicity attained by surface treatment will be sustained depending on factors like the temperature and humidity of the environment in which the PDMS mold is preserved [25]. Figure 2.10 show the plasma treatment equipment used for experiment.

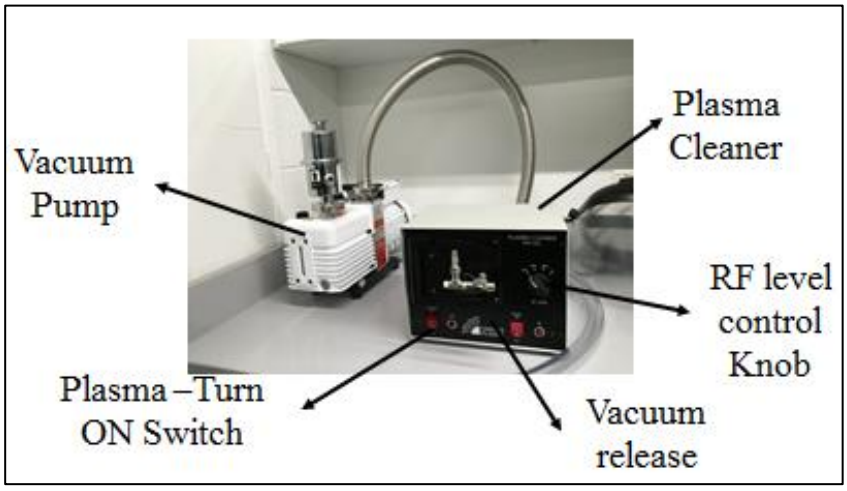

Figure 2.10 Oxygen plasma treatment equipment.

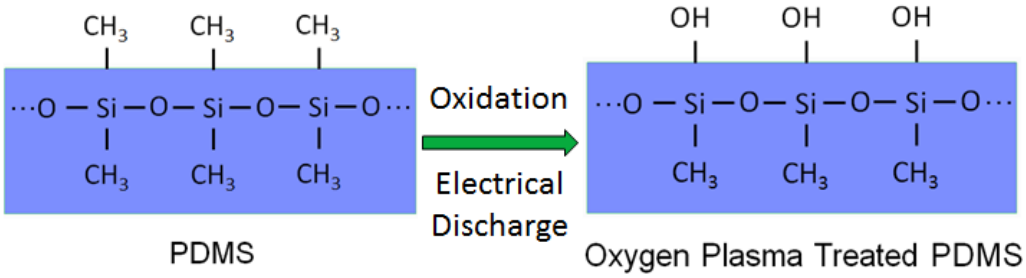

Figure 2.11 Schematic of Plasma treatment

The oxygen plasma treatment of the PDMS introduces polar functional groups such as the Silanol groups (SiOH) on the surface of the PDMS. The silanol groups are

responsible for converting the PDMS property from hydrophobic to hydrophilic as shown in Figure 2.11. The oxygen plasma treatment also helps in increasing the adhesion property of the PDMS, so that it can be easily bonded with other substrates or another PDMS slab. However, the surface treatment due to Oxygen plasma treatment is not permanent. PDMS regains its hydrophobicity after a certain period approximately 6 hours [28].

In order to convert the PDMS to hydrophilic in nature, the PDMS is exposed to oxygen plasma for various durations. In this experiment the hydrophilicity of PDMS is measured with respect to variation in duration of the plasma treatment. All plasma treatments are conducted on the 'Plasma Cleaner PDC-32G with an oxygen flow rate of 20 sccm and 100 bar pressure. A radio frequency (RF power supply of 150W) of 13.56 MHz is used for plasma excitation.

2.3 Capacitance based Sensing Mechanism using the Gold Interdigitated Electrodes

In microfluidic biochip, the gold nano interdigitated electrodes (IDE) are fabricated at different sections of the microchannel to sense the biological reactions at multiple locations of microchannel, in order to multiply the sensing mechanism and enhance the detection sensitivity. The gold nano IDEs are connected to individual contact pads so that the signal from each IDE can be separately monitored. A specific antibody can be immobilized at a specific IDE so that the concentration of the corresponding antigens can be detected by the antigen-antibody complex formed at

that IDE. Detection of concentration of each individual antigen in the biofluid sample can enhance the detection specificity.

2.3.1 Fabrication of gold electrodes on Si wafer

The Silicon wafer is cut as per the dimensions desired and cleaned with isopropanol before starting the electrode fabrication. The Silicon wafer is then Spin coated with positive tone photoresist. The photoresist used is PMMA-A6. The desired thickness of electrodes is 100nm. Ideally, the height of the PMMA deposits should be more than 3 times the height of the electrodes. The soft baking of the Silicon wafer is performed on a hot plate at around 180° C for 120 seconds. The coated Silicon wafer then undergoes Electron beam Lithography procedure as per the CAD model provided for the EBL machine. The desired pattern (Interdigitated) is formed on top of the coated Silicon wafer. The patterned Si wafer is then developed with MIBK:IPA for 60s and washed with IPA for another 60s and then dried with Nitrogen gas.

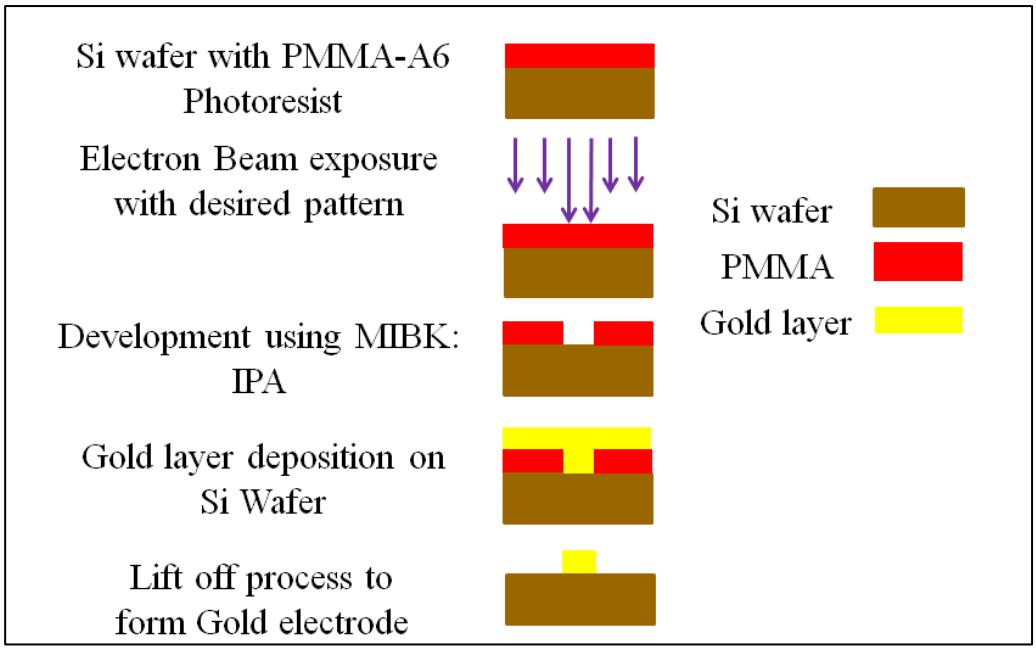

Figure 2.12 Schematic of various steps in the nano electrode fabrication.

The Silicon wafer is placed in a Physical vapor deposition PVD machine for deposition of metal on the wafer. A layer of Titanium (approx.10nm) is deposited on the patterned grooves of the chip. This is done to improve the adhesion of gold on Silicon. Gold is deposited over the wafer by high vacuum evaporator (Kurt J Lesker PVD-75 Evaporator). A approximately 90nm of Gold is deposited on top of the Si wafer. The lift-off process is performed by removing the positive tone photoresist by cleaning the wafer in Acetone Ultrasonic bath for 3 minutes and then thoroughly rinsed with Isopropanol in order to prevent redeposition. The fabricated wafer with gold deposition is then rinsed with distilled water and dried with Nitrogen gas. The electrodes are fabricated by following the fabrication steps as shown in Figure 2.12. Figure 2.13 show the atomic force microscopic image of the interdigitated electrodes fabricated for the experiment.

2.4 PDMS Mold Attachment to Si-Wafer with the Sensing Platform

The PDMS microchannel was closed with the Si-wafer with interdigitated electrodes, so that the microchannel has 3 sides with PDMS surface and one side with Si-wafer surfaces with sensing platform with the aid of alignment pins. The plasma treated pdms mold is carefully aligned to the Si wafer with nano interdigitated electrodes immobilized with the antibodies as shown in Figure 2.1. The immobilizations of the antibodies are discussed in detail in next chapters.

CHAPTER 3

SENSITIVITY STUDY OF INTERDIGITATED ELECTRODES UNDER MIROFLUIDIC FLOW CONDITION DURING DETECTION OF BIOMARKER (CA125ANTIGEN)

3.1 Materials and Experiments

3.1.1 Chemicals and Apparatus

Silicon Wafer (Si), Thiourea (CH_4N_2S), Phosphate buffer saline (PBS), Glutaraldehyde ($C_5H_8O_2$) was purchased from Sigma Aldrich (USA). The Polydimethylsiloxane (PDMS sylgard 184) base and curing agent were purchased from Dow Corning (USA). The CA-125 monoclonal antibodies and the CA-125 antigens were bought from Meridian Life Science. Signatone-Probe station was used for electrical measurements. Bruker Atomic Force Microscope is used for AFM images.

3.1.2 Immobilization of CA-125 Antibodies on Interdigitated Electrodes

The gold interdigitated electrodes on Si-wafer were washed for 3 times with ethanol and de-ionized water and dried with the Nitrogen gas. Then the electrodes were immersed in a 50mM Thiourea solution (CH_4N_2S) and incubated for 12 hours to form the SAM layer Self-assembled Monolayer (SAM layer). To remove the excessive Thiourea solution, the surface of the electrode was rinsed with ethanol and Millipore deionized water and then dried using Nitrogen gas. The electrical insulation of the SAM layer was confirmed by evaluating the short circuit/current leakage using the 2 point probe station. Glutaraldehyde ($C_5H_8O_2$) was used to promote the surface activation on the SAM layer, for enhanced antibody binding to

the electrodes.

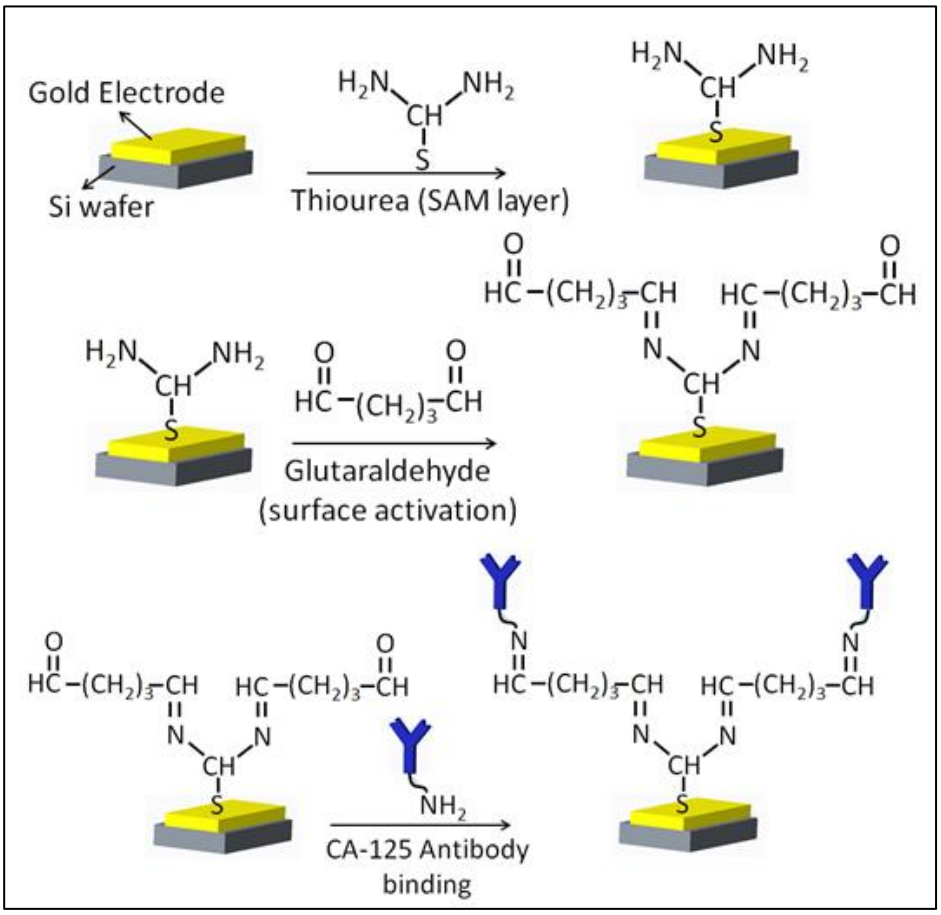

Figure 3.1 Schematic diagram of CA-125 immobilization on top of the gold electrodes.

The CA-125 antibodies were immobilized on the gold interdigitated electrodes by incubating the electrodes with 0.5ul of 7mg/ml CA-125 antibodies in Phosphate-buffered saline (PBS) solution for 2 hours at 4˚C. A 10mM of 1-dodecanthiol in ethanolic solution was added on top of the SAM coated electrodes to block the unwanted sites or the bare spots on electrode surface for 1 hour [20-23]. Thus the CA-125 antibodies were immobilized on the gold interdigitated electrodes on Si-wafer as shown in Figure 3.1. The consistency of the antibodies immobilization on the electrodes for all the experiments and at all the iterations was

verified using the surface characterization and electrical measurements (will be explained in detail in 'results and discussion' section), in order to maintain uniform sensing conditions.

3.1.3 Biofluid sample-CA 125 Antigens Solution

The biofluid sample is the 55 ug/ml of CA-125 antigens concentration in PBS solution at pH 7.4. The biofluid sample is passed on the immobilized antibodies on the electrodes, to form antigen –antibody interaction as shown in Figure 3.2

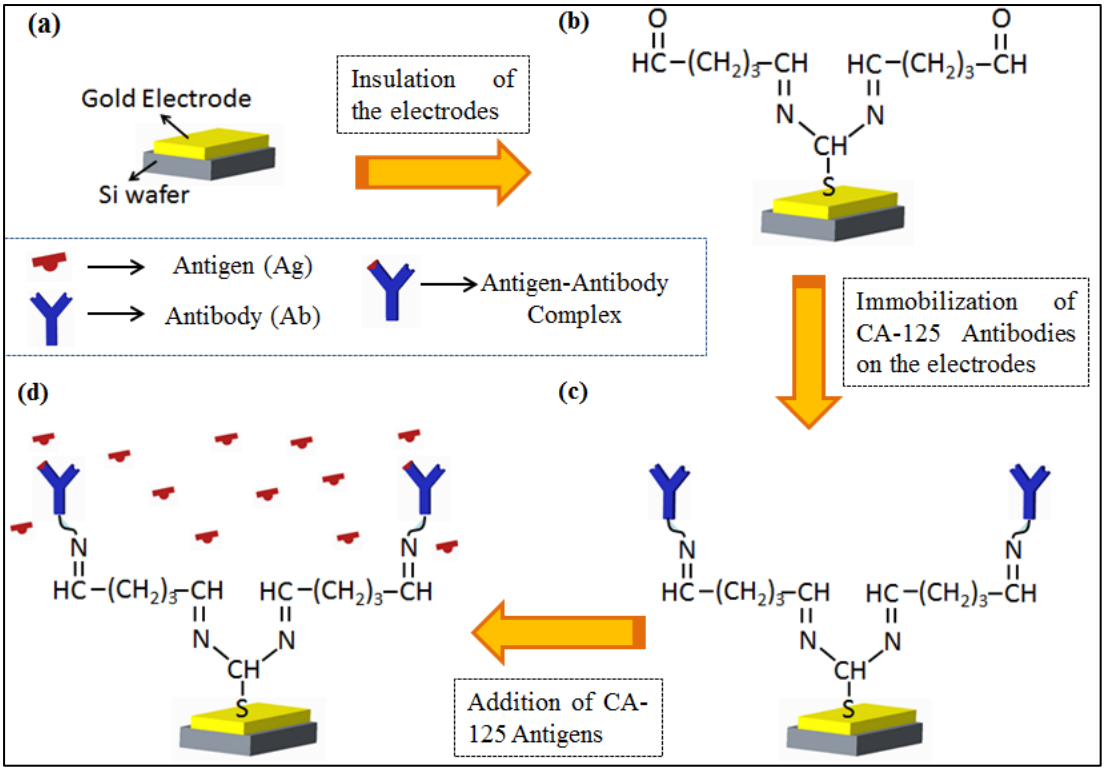

Figure 3.2 Schematic of key steps implemented to setup the experiment of biosensing (a) gold interdigitated electrodes on the Si-wafer (b) insulation of the electrodes using the surface activated SAM layer (c) CA-125 antibodies immobilization (d) CA-125 antigens binding with the immobilized antibodies on electrodes.

3.1.4 Electrical Measurements

The capacitance measurements were made at two stages: **Stage -1**: During the

different layers of biosensor fabrication (like bare electrodes, insulated electrodes with SAM layer, and electrodes with CA-125 antibodies). **Stage-2**: During the antigen-antibody interaction 'with' and 'without' microfluidic flow conditions. The electrical measurements in this experiment were measured using the Signatone 2 point probe station and with Agilent 4284A Precision LCR meter as show in Figure 3.3. The LCR meter readings were processed using LabVIEW NI 488.2 version software to plot the data. The targeted frequency range was between 10 kHz and 100 kHz with a step of 10 kHz at every succession. Each capacitance measurement was done at 100mV amplitude.

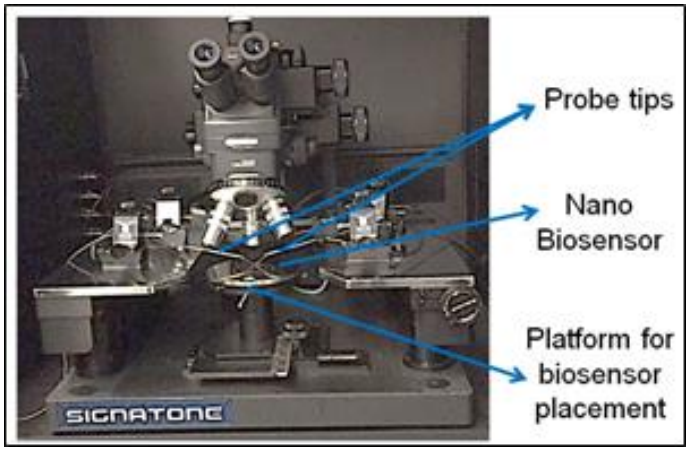

Figure 3.3 Image of the Signatone probe station used for capacitance measurements

3.2 Results and Discussion

3.2.1 Capacitance of the Interdigitated Electrodes

The interdigitated electrodes generate the electric field to produce the capacitance and used for capacitive measurements. The interdigitated electrode facilitates higher effective area with the same volume or space which significantly reduces the cost sensing setup [29-31].The range of electric field generated by the interdigitated

electrodes fabricated in this experiment were in nano scale, which stays exactly in the range of interest as the scale of antigen and antibodies also lies in the nanoscale [32-37]. The electrical properties of the interdigitated electrodes such as conductivity, permittivity, capacitance and impedance can be studied with the information of the dielectric properties of the medium between the electrodes. The size of the electric field lines generated by these interdigitated electrodes depends on the geometry and configuration of the electrodes, dielectric medium and the electrical inputs.

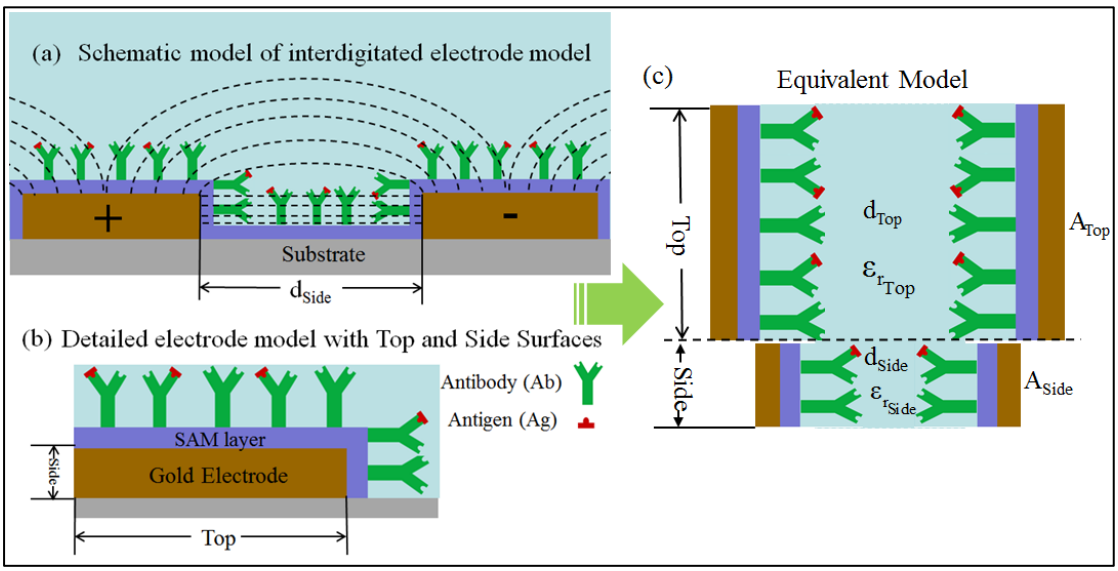

Figure 3.4 (a) Schematic of the interdigitated electrode model with active 'Top' and 'Side' surfaces and (b) The detailed electrode model of (figure-3.4(a)) with 'Top' and 'Side' surfaces of electrode. (c) Equivalent model with the single surface model for both 'Top' and 'Side' of electrode.

The effective surface area of the electrode which effect the capacitance are, 'Top' surface area and 'side' surface are as shown in the Figure 3.4 (a). The net capacitance of the electrode model ' $C_{Electrode\ model}$ ' can be measured by eq(1) with the combined capacitance of the 'Top' and 'Side' surface of the electrode. The

capacitance of the 'Top' surface of the electrode can be calculated by the integrating the capacitance of the infinitesimal area over the surface area as,

$$C_{\text{Electrode model}} = \int \varepsilon_{r_{\text{Top}}} \cdot \varepsilon_o \cdot \left(\frac{dA_{\text{Top}}}{d_{\text{Top}}} \right) + \varepsilon_{r_{\text{Side}}} \cdot \varepsilon_o \cdot \left(\frac{A_{\text{Side}}}{d_{\text{Side}}} \right) \quad \text{(eq1)}$$

where $\varepsilon_{r_{\text{Top}}}$ & $\varepsilon_{r_{\text{Side}}}$ is the relative permittivity of the medium on the top and side surfaces of the electrode, ε_o is the vacuum permittivity, A_{Top} & A_{Side} are the effective surface areas on the 'Top' and 'Side' surfaces of the electrode, and 'd_{Top}'& 'd_{Side}' are the effective distances between the top and side surfaces of the electrodes.

By assuming that the SAM and Antibody layers are homogenous on the surface of electrode, the capacitance of the 'Electrode model' can be measured with the 'Equivalent model' as shown in Figure 3.4(c),

$$C_{\text{Equivalent Model}} = \varepsilon_{r_{\text{Top}}} \cdot \varepsilon_o \cdot \left(\frac{A_{\text{Top}}}{d_{\text{Top}}} \right) + \varepsilon_{r_{\text{Side}}} \cdot \varepsilon_o \cdot \left(\frac{A_{\text{Side}}}{d_{\text{Side}}} \right) \quad \text{(eq2)}$$

With the physical approximation of the relative permittivity of the medium on the surface of the electrode are directly proportional to the ratio of corresponding surface area and effective distance as shown below eq3,

$$\varepsilon_{r_{\text{Top}}} : \left(\frac{A_{\text{Top}}}{d_{\text{Top}}} \right) = \varepsilon_{r_{\text{Side}}} : \left(\frac{A_{\text{Side}}}{d_{\text{Side}}} \right) = \varepsilon_{r_{\text{eff}}} : \left(\frac{A_{\text{eff}}}{d_{\text{eff}}} \right) \quad \text{(eq3)}$$

the equivalent model is approximated to the Simplified model as shown in Figure 3.5 The capacitance of the simplified model can be calculated as per eq4,

$$C_{\text{Simplified Model}} = \varepsilon_{r_{\text{eff}}} \cdot \varepsilon_o \cdot \left(\frac{A_{\text{eff}}}{d_{\text{eff}}} \right) \quad \text{(eq4)}$$

Where $\varepsilon_{r\,eff}$ the relative permittivity of the medium between the electrodes is, ε_0 is the vacuum permittivity, A_{eff} is the effective surface area and d_{eff} is the effective distance between electrodes.

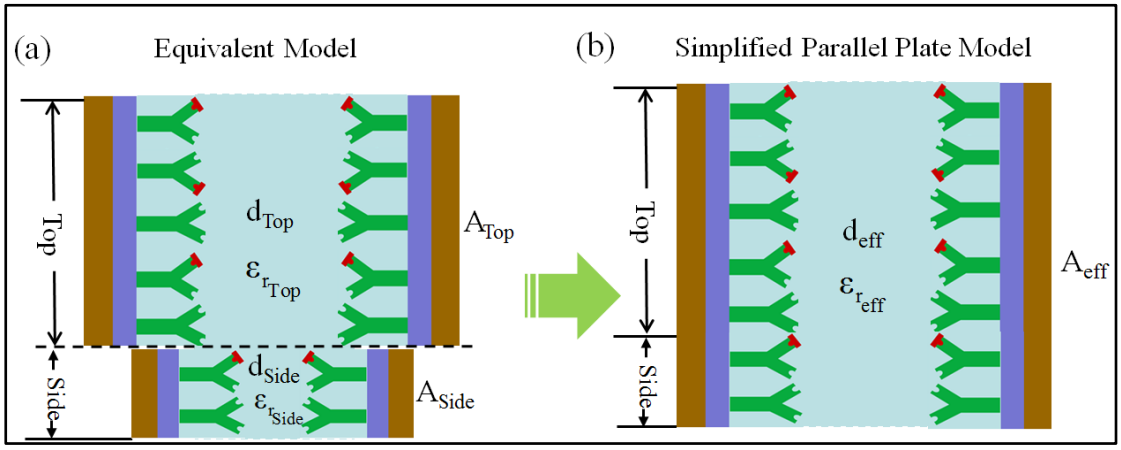

Figure 3.5 Schematic of (a) Equivalent model with the single surface model for both 'Top' and 'Side' of electrode (b) Simplified parallel plate model from the equivalent model of the electrode.

Where,

$$A_{eff} \approx A_{Side} + A_{Top} \qquad \text{(eq3)}$$

$$d_{eff} \approx \frac{A_{eff}}{\frac{\varepsilon_{r_{Top}}}{\varepsilon_{r\,eff}}\left(\frac{A_{Top}}{d_{Top}}\right) + \frac{\varepsilon_{r_{Side}}}{\varepsilon_{r\,eff}}\left(\frac{A_{Side}}{d_{Side}}\right)} \qquad \text{(eq4)}$$

$$\varepsilon_{r\,eff} \approx \varepsilon_{r_{Side}} + \left[\varepsilon_{r_{Top}} - \varepsilon_{r_{Side}}\right]\left[\frac{\left(\frac{A_{eff}}{d_{eff}}\right) - \left(\frac{A_{Side}}{d_{Side}}\right)}{\left(\frac{A_{Top}}{d_{Top}}\right) - \left(\frac{A_{Side}}{d_{Side}}\right)}\right] \qquad \text{(eq4)}$$

With the necessary experimental conditions, if $\varepsilon_{r\,eff}$ can be assumed as,

$$\varepsilon_{r\,eff} \approx \varepsilon_{r_{Top}} \approx \varepsilon_{r_{Side}} \qquad \text{(eq5)}$$

Then the d_{eff} can further be simplified as,

$$d_{eff} \approx \frac{A_{Side} + A_{Top}}{\left(\frac{A_{Side}}{d_{Side}}\right) + \left(\frac{A_{Top}}{d_{Top}}\right)} \quad \text{(eq6)}$$

3.2.2 Microfluidic Flow Condition

In this experiment, the microchannel with the width of 'w' (300 um) and of depth 'h' (107um) was employed to generate the microfluidic flow on the sensing platform as shown in Figure 3.6 (a). The biofluid flow in the microchannel generates a shear on the sensing surface. The shear rate is defined by the change in the biofluid flow velocity (U_x) with respect to the microchannel height at the microchannel surface (y=0) and it is calculated by applying the boundary conditions of poiseuille flow in the infinite parallel plates due to the high aspect ratio and insignificant side wall effect as shown below [23] as,

$$\tau = \mu \left.\frac{\partial U_x}{\partial y}\right|_{y=0} \approx \mu \frac{6Q}{wh^2} \quad \text{(eq7)}$$

Where Q is the flow rate of the biofluid which is measured as 0.2 uL/sec. Thus the shear stress (τ) is calculated as 0.307 Pa with the microchannel of width 300um and depth of 107um. The dynamic viscosity of the biofluid sample for calculating shear stress was (0.00088 pa.sec). The shear stress influence on the stability of the immobilized CA-125 antibodies on the sensing surface and the corresponding effect on sensitivity of the antigen-antibody interaction is explained in detail in further sections). Figure 3.6(b) is the microscopic image during the biofluid flow in microchannel.

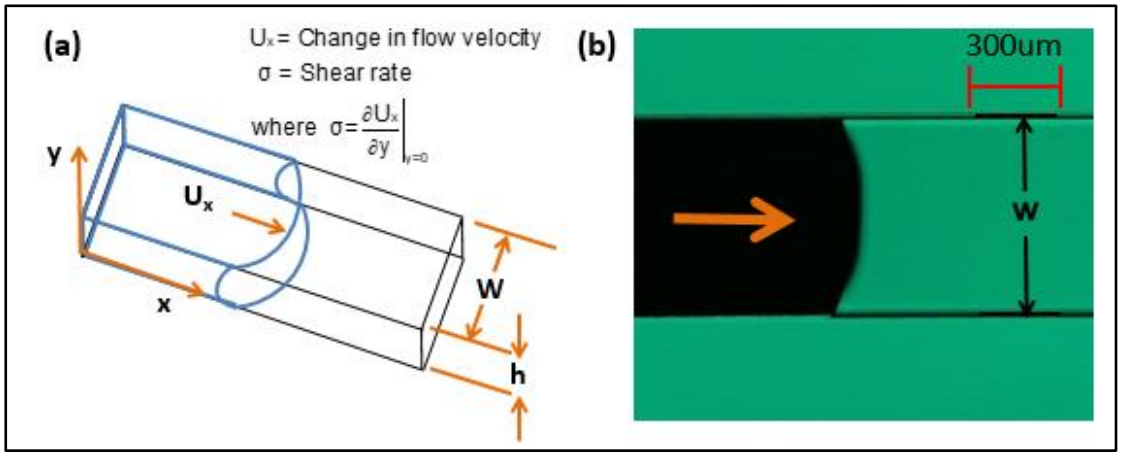

Figure 3.6 Schematic of the microchannel with the shear rate measurement. (b) The image of the microchannel during the flow of biofluid sample.

3.2.3 Surface Characterization

The modification of the silicon substrate with each layer of sensing platform was validated using the AFM measurements. AFM images were taken to confirm the fabrication of interdigitated electrodes, SAM layer on the interdigitated electrodes and CA-125 antibody immobilization on the electrodes. In figure-3.7(a), the relatively smooth surface of the bare electrodes when compared to the surface with SAM layer on the electrodes (as shown in figure-3.7(b)) was observed. When the CA-125 antibodies were immobilized on the electrodes with SAM layer (as shown in figure 3.7 (c)), a more rough surface morphology was observed when compared to the SAM layer on the electrode (as shown in Figure-3.7 (b)). The increase in height of the electrode surface from 90 nm to 110 nm after the SAM layer fabrication on the electrode provides the evidence of formation of the SAM layer on the electrode. The increase in the net height of the electrodes and surface roughness confirms the formation of the SAM layer and immobilized antibody layer on the

bare electrodes. The capacitive measurements additional to AFM image confirm the SAM layer insulation and the antibodies immobilization on the electrodes.

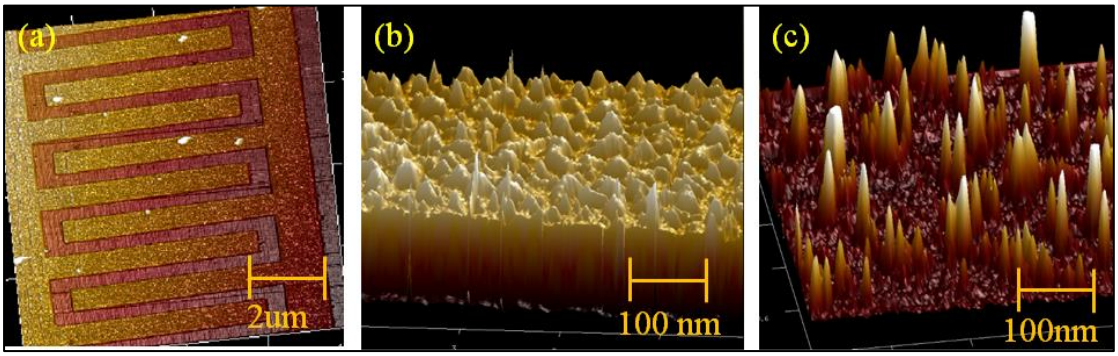

Figure 3.7 AFM images of the surface of the interdigitated electrodes with Bare electrodes (left), SAM layer (middle) and immobilized antibodies (Right).

3.2.4 Electrical Characterization

The capacitance measurements were performed at different stages of the experiment to study the influence of microfluidic flow on the sensing mechanism. The electrical measurements were performed at two stages. Stage-1: During the fabrication of the sensing platform in order to validate the functionality of the each layer of the sensing platform. Stage-2: During the antigen- antibody interaction with static drop condition and with microfluidic flow of CA-125 antigens on the sensing platform in order to study the influence of microfluidic flow on sensitivity.

Stage-1: Capacitance measurement at different layers of sensing platform: The capacitance measurements were taken at each modification of the Si-substrate at different layers of the sensing platform. The Figure 3.8 shows the plot of capacitance variation with frequency for bare electrodes, insulated electrodes with SAM layer, and electrodes with immobilized CA-125 antibodies. The capacitance at the bare electrodes was measured by connecting the probes of electrical analyzer, to

the contact pads of the interdigitated electrodes as 9.12 pF at 10 kHz and 8.59 pF at 100 kHz. Similarly, the capacitance of the insulated electrodes with the SAM layer was measured from the contact pads of electrodes coated with SAM layer, as 9.20 pF at 10 kHz and 8.53 pF at 100 kHz. The LCR meter measures the impedance of the net circuit and converts that into capacitance measurement based on the real and imaginary parts of impedance. The higher electron transfer resistance of the SAM layer on the electrodes directly influences the real part of the impedance. The increment in the resistance causes the increment in the net impedance. As a result, the net capacitance of the insulated electrodes with SAM layer has shown lower values when compared to the bare electrode capacitance over the frequency.

After the immobilization of the CA-125 antibodies on the surface activated SAM layer of the electrodes, the capacitance at the immobilized antibodies layer were measured. The measurements were taken by connecting the electrical analyzer probes to the contact pads of the electrodes with immobilized CA-125 antibodies. The capacitance measurement at the immobilized CA-125 antibody layer was 18.76 pF at 10 kHz frequency and then reduced to 11.29 pF at 100 kHz frequency as shown in figure-3.8.

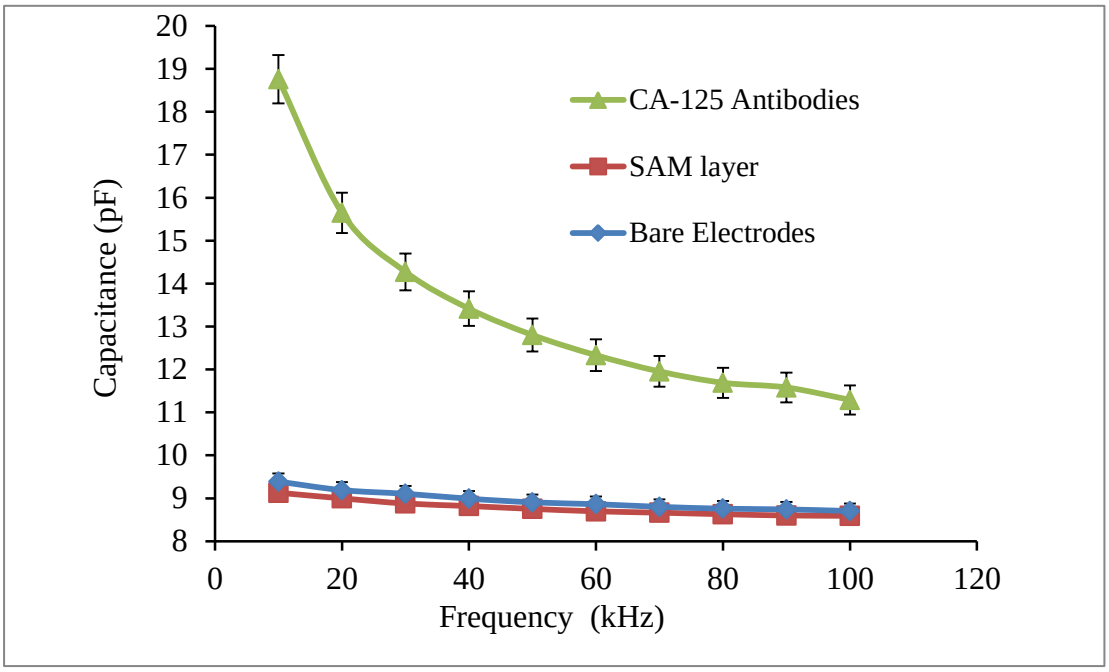

Figure 3.8 Plot of capacitance measurements with frequency for bare electrodes, insulated electrodes with SAM layer, and electrodes with CA-125 antibodies.

Stage-2: Capacitance measurements during the Antigen-Antibody interaction with 'static drop' and 'microfluidic flow' of the CA-125 antigens: The capacitance measurements were taken during the CA-125 antigen-antibody interaction with static drop of biofluid sample and with microfluidic flow if biofluid sample. The Figure 3.8 shows the curves plotted between the capacitance variation and frequency when the antibodies interact with antigens at different conditions such as biofluid (CA-125 antigen in buffer solution) as static drop, PBS solution (without any antigens) with microfluidic flow, and biofluid (CA-125 antigen in buffer solution) with microfluidic flow.

Static drop condition of biofluid sample with CA-125 antigens: The biofluid sample with CA-125 antigens was placed as a drop of 0.5ul on the sensing platform that was immobilized with the CA-125 antibodies. The capacitance values of the CA-125

antigen- antibodies layer are taken by connecting the measured by electrical analyzer probes to the contact pads of the electrodes during the antigen-antibody interaction. The capacitance values when the biofluid sample is placed on the sensing platform at the stationary drop condition during the CA-125 antigen-antibody interaction was measured as 296.09 pF at 10 kHz frequency and then lowered to 110.92 pF at 100 kHz frequency as shown in Figure 3.8. The CA-125 antigen-antibody interacts are highly selective and specific. The change in the net molecular size due to CA-125 antigen/antibody complex formation creates a disturbance in the distribution of charges, and creates a dipole moment at the dielectric interface of sensing surface. The hydrocarbon chains present in the proteins are polar in nature [29-31]. The net charge variation due to the interaction of the hydrocarbons of antibodies and antigens creates a process of local polarization that directly influences the dielectric permittivity of the antigen/antibody complex on the electrode surface. The dipole-dipole interaction stimulates the polarization on the electrode surface. The dielectric of each antigen/antibody complex has unique characteristic over the range of frequencies. At the high frequencies, the charge accumulation period for the capacitor is much less, when compared to the lower frequencies. Due to the low charge accumulation period of capacitor, the capacitance measurement is lower at higher frequencies than when compared to capacitance measurement at lower frequencies. So the capacitance measurement of CA-125 antigen-antibody interaction has decreased from 296.09 pF to 110.92 pF

with frequency change from 10 kHz to 100 kHz as shown in figure-3.8.

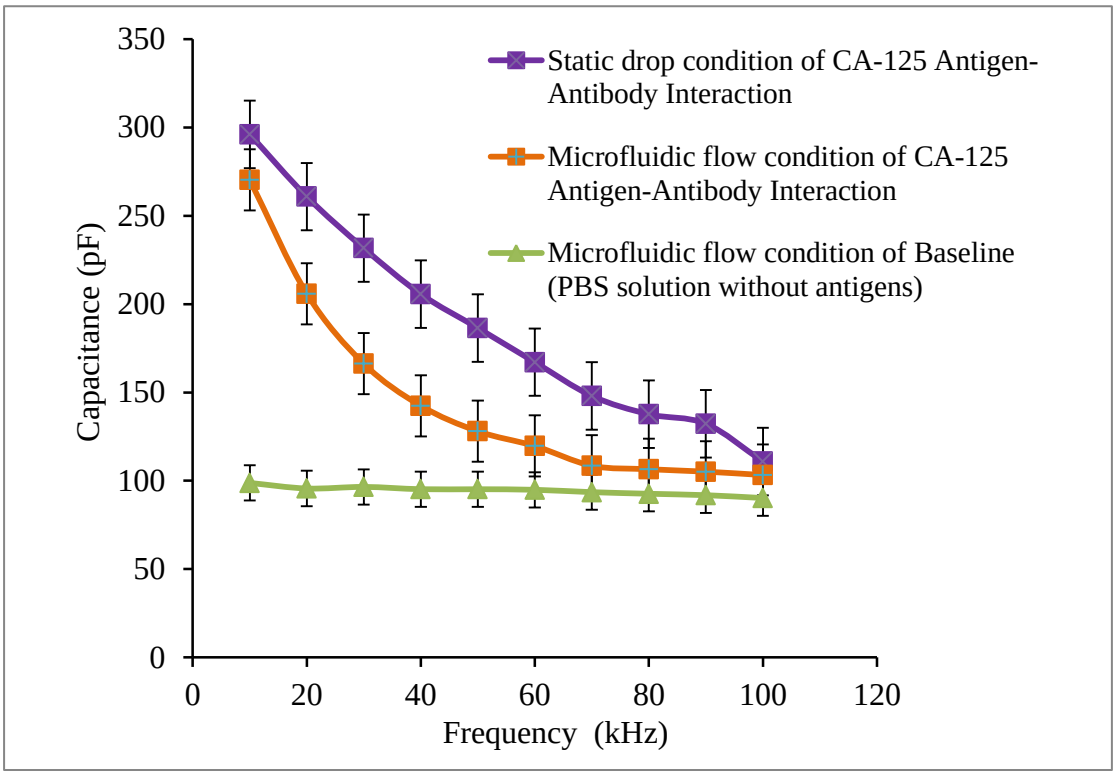

Figure 3.9 Plot of Capacitance measurements with frequency for Baseline (PBS solution without antigens),biofluid sample during microfluidic flow and biofluid sample without microfluid flow.

Microfluidic flow condition of the PBS without antigens: The sensing platform was enclosed with PDMS microchannel (the specifications of the microchannel were already discussed in the earlier sections). All fluids (buffer solution and biofluid sample) were passed through the microchannel of same dimensions and at a constant flow rate (0.25uL/sec) to employ the same microfluidic flow in all the experiments and at all the iterations. As the initial step, the phosphate buffer saline (PBS) solution has been passed through the microchannel and the capacitance measurements were taken during the flow and it is regarded as Baseline. The capacitance values were measured as 98.78 pF at 10 kHz frequency and slowly

decreased to 90.23 pF at 100 kHz frequency as shown in figure-3.9. It was observed that the capacitance measurements almost remained unchanged over the frequency changes. In the Baseline measurements, the CA-125 antigens were not present in the PBS solution, so the capacitance change from the antibody layer of 18.76 pF at 10 kHz to baseline layer of 98.78 pF at 10 kHz is purely attributed to the change in dielectric properties of the medium without any antigen-antibody interactions.

Microfluidic flow condition of the biofluid sample with CA-125 antigens: To understand the sensitivity variation due to the microfluidic flow, the biofluid sample with exact same sensing composition (to that of static drop condition) were passed through the microchannel at a constant flow rate (0.25uL/sec) on the sensing platform. The capacitance values were measured during the antigen-antibody interaction when the biofluid was flowing in the microchannel. The capacitance measurement in the microfluidic flow condition during CA-125 antigen-antibody interaction was measured as 270.34 pF at 10 kHz frequency and gradually decreased to 103.25 pF at 100 kHz frequency as shown in figure-3.9. The increase in the capacitance measurement during the microfluidic flow of PBS solution without antigens (98.78 pF at 10 kHz) and biofluid sample with antigens (270.34 pF at 10 kHz) caused due to the CA-125 antigen-antibody interaction during the microfluidic flow. The capacitance measurement during the CA-125 antigen-antibody interaction has decreased from 296.09 pF to 270.34 pF at 10 kHz when compared to static drop condition and microfluidic flow condition as shown in figure-3.9

The tight confinement of the biofluid flow microfluidic exerts high surface shear stress which can impact the stabilization of the antibodies that are immobilized to the sensing platform [33 & 34]. The shear forces applied by the fluid on the antibodies that are binded to the electrode of sensing platform in microchannel induce mechanical breakage of the weak bonds of the antibodies with the electrode [35]. The possible breakage of bonds of the antibodies with the sensing surface could influence the instability of the immobilization of antibodies. So due to existence of shear in the microfluidic flow condition, the stability of the CA-125 antibody would be significantly lower that could directly influence the sensitivity. Therefore the capacitance measurement of the antigen- antibody interaction is lower in the microfluidic flow condition when compared to static drop condition.

3.3 Conclusions

In the current study, the sensitivity variation of the biosensor with interdigitated electrodes due to microfluidic flow was established by detecting the CA-125 antigens from biofluid. As per the experimental results, the following conclusions can be made:

(1) The sensing platform layers were successfully fabricated and the functionality of each layer is individually validated with the electrical signal responses.

(2) The Cancer Antigens (CA-125) are successfully immobilized using the chemical treatments with Thiourea and Glutaraldehyde.

(3) The cancer antigens CA-125 are detected from the biofluid sample using the interdigitated electrodes in the biochip in the static drop condition and also in microfluidic flow condition.

(4) The capacitance measurement of the biosensor with microfluidic flow condition is lower than static drop condition during the detection of CA-125 antigens using the interdigitated electrodes.

CHAPTER 4

SENSITIVITY STUDY OF GOLD NANO PARTICLES ON INTERDIGITATED ELECTRODES WITH MIROFLUIDIC FLOW CONDITION DURING DETECTION OF BIOMARKER (CA125 ANTIGEN)

4.1 Materials and Methods

4.1.1 Chemicals and Apparatus

Thiourea (CH_4N_2S), Phosphate buffer saline (PBS), 1-ethyl-3-(-3-dimethylaminopropyl) carbodiimide (EDC), N-hydroxysuccinimide (NHS), Carboxy functionalized (Lipoic acid) Gold nanospheres were purchased from NanoComposix (USA). The CA-125 monoclonal antibodies and the CA-125 antigens were bought from Meridian Life Science. The Polydimethylsiloxane (PDMS) base and curing agent were bought from Fisher Scientific.

4.1.2 Immobilization of CA-125 Antibodies on Interdigitated Electrodes with Gold Nanoparticles

The interdigitated gold electrodes were washed multiple times with ethanol and de-ionized water and dried with nitrogen gas before addition of the SAM layer. The interdigitated gold electrodes surface was coated with Self Assembled Monolayer (SAM) by incubating the sensor in 50mM Thiourea solution overnight. The interdigitated electrodes were rinsed with ethanol and de-ionized water and dried with nitrogen gas. The formation of the SAM layer was confirmed using two point electrical probe station. Furthermore, the AFM image of the electrodes confirmed the formation of the SAM layer. The carboxylic encapsulated gold nanoparticles having 5nm size were incubated on the surface of the SAM modified sensor for 10 h.

After the incubation step, the gold nanoparticles surface was activated using 50mM of EDC and NHS. This process enables the antibodies to attach covalently to the carboxylic gold nanoparticles [44-47]. The surface activation of the carboxylic gold nanoparticles is shown in Figure 4.1

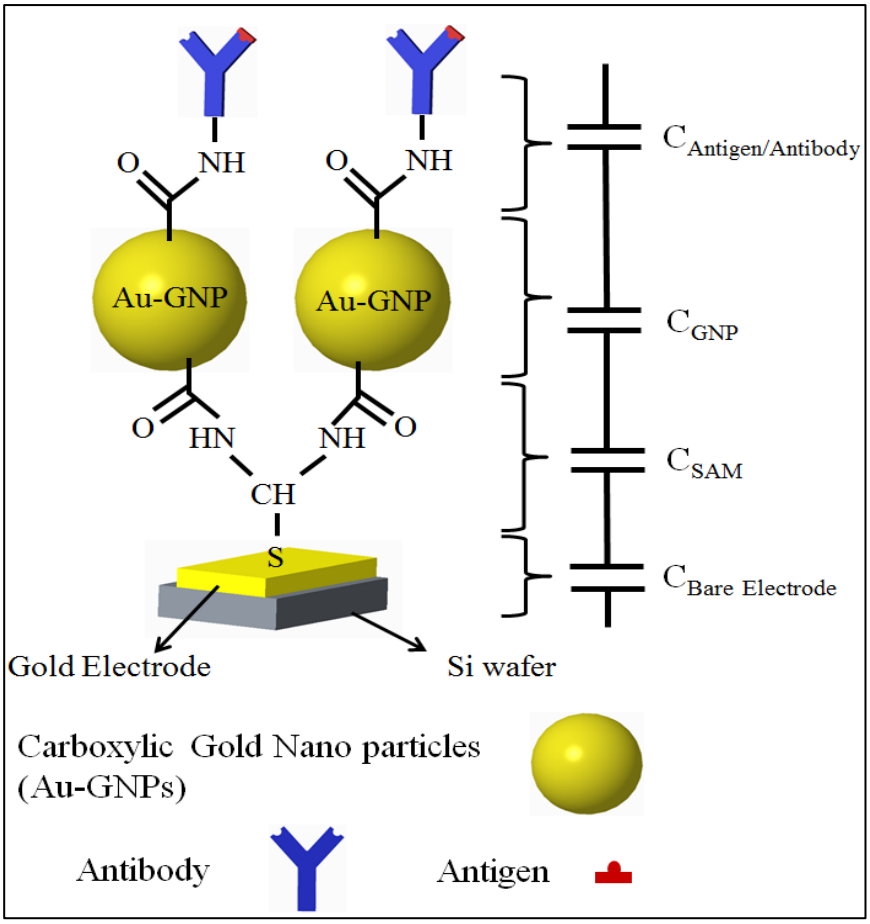

Figure 4.1 Schematic diagram of CA-125 immobilization on top of the gold electrodeswith gold nano particles.

The sensor surface was washed using PBS solution and dried with Nitrogen gas for removal of excess of unwanted gold nanoparticles. Following this step, the CA-125 antibodies were immobilized on top of the surface activated gold nanoparticles based sensor by incubating it with 0.5 µl of 7mg/ml CA-125 antibodies in PBS solution for 2 hours. The incubation step took place at 4˚C. The

sensor surface was rinsed using PBS solution and the non-reacted groups on the sensor surface were blocked by addition of approximately 1µl of ethanolamine on top of the modified sensor for 1h. The sensor was further cleaned with PBS and de-ionized water as shown in Figure 4.2.

4.1.3 Biofluid sample-CA 125 Antigens Solution

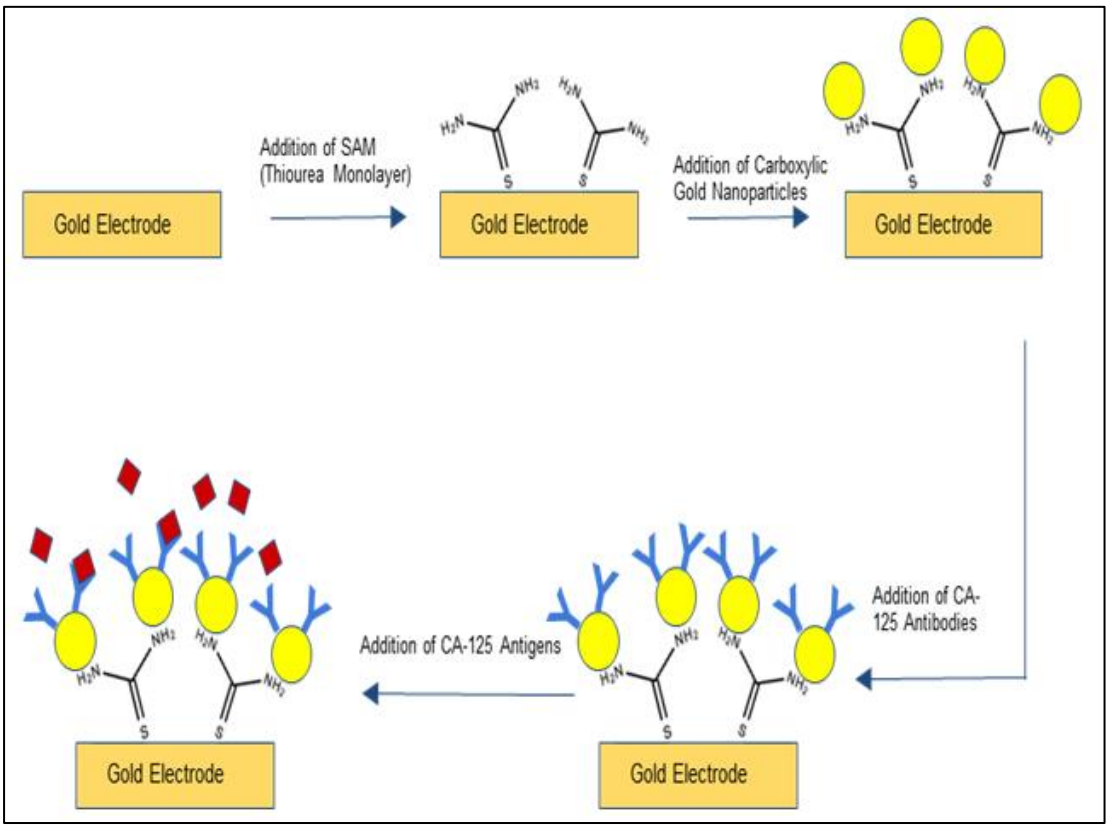

Figure 4.2 Schematic of key steps implemented to setup the experiment of biosensing.

The biosensor is based on dynamic conditions and hence it is integrated with the hydrophilic PDMS microfluidic channel on top of it. The PDMS microchannel is prior treated with oxygen plasma to make it hydrophilic ‘w’ (515 um) and of depth ‘h’ (107um). An approximate of 5µL drop of CA-125 antigens solution with 56µg/ml concentration was placed on the inlet of the microchannel. The antigens

solution flows very quickly through the hydrophilic microchannel and interacts with the antibodies which are exposed on the sensor platform due to the capillary effect. Figure 4.2 shows the schematic key steps in the biosensing mechanism of CA-125 antigens from biofluid.

4.1.4. Electrical Measurements

All the electrical measurements in this experiment were taken using two point probe station and the capacitance were measured by Agilent 4284A Precision LCR meter. The selected frequency range was between 10 kHz and 100 kHz with a step of 10 kHz at each succession. The capacitive values were measured for (a) bare electrodes, (b) after insulation of the electrodes by SAM layer; (c) after addition of carboxylic functionalized gold nanoparticles or non-carboxylic gold nanoparticles, (d) after the immobilization of the CA-125 antibodies and (e) after conjugation of CA-125 antigens and antibodies when antigens solution flows through the microchannel. All the capacitive measurements were done at 100mV amplitude with the DC voltage at 0.5V during this experiment.

4.2 Results and Discussion

4.2.1 Surface Characterization

In this experiment, the purpose of the SAM layer is to insulate the electrodes and prevent it from short circuiting [48]. The functionality and the presence of the SAM layer are confirmed by AFM image of the Thiourea coated gold electrodes. Figure 4.3 shows the AFM image of the electrodes having Thiourea layer deposited on top of it. The increment in the net vertical height of the electrodes along with the surface

roughness confirms the formation of the SAM layer. The electrical measurement additionally confirms the SAM layer insulation on the surface of the electrodes.

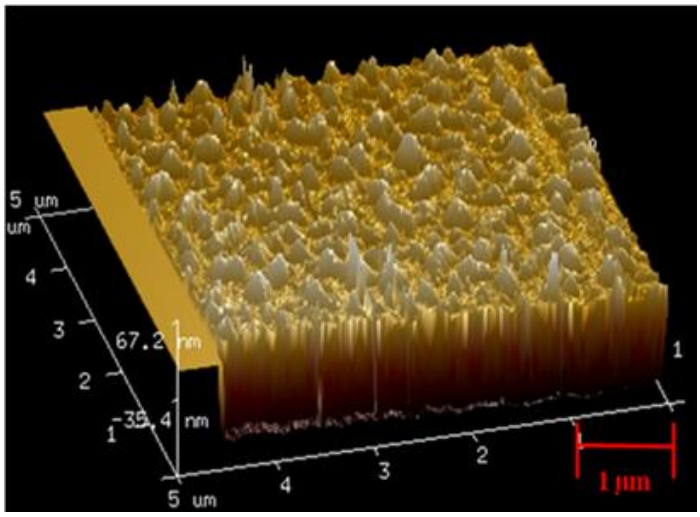

Figure 4.3 The AFM image of the interdigitated gold electrode coated having SAM layer deposited on top of it.

The Carboxylic functionalized gold nanoparticles were incubated and surface activated using EDC/NHS coupling. The CA-125 antibodies are then added and incubated on top of the gold nanoparticles. Figure 4.4 shows the AFM images of the gold nanoparticles and the antibodies present on top of the gold nanoparticles.

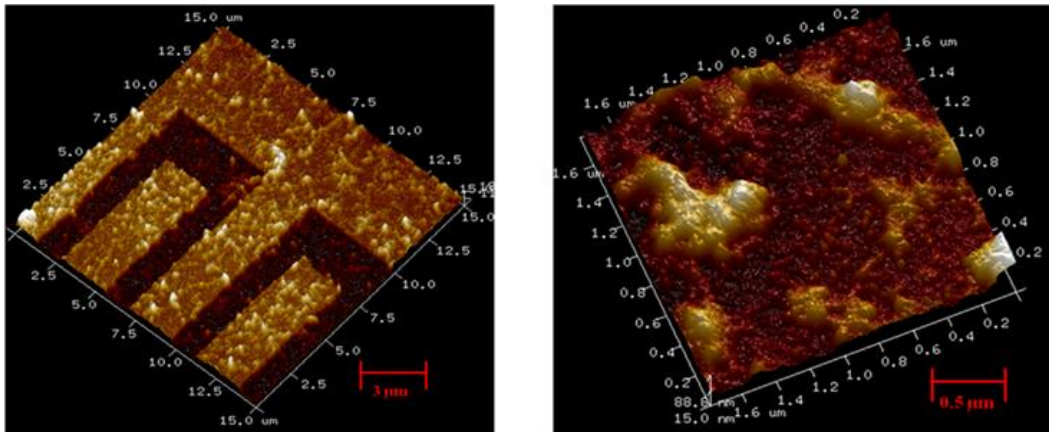

Figure 4.4 AFM images of the Gold nanoparticles present on top of gold electrodes (LEFT) and the CA-125 antibodies present on top of the Gold nanoparticles in the sensor platform (RIGHT)

4.2.2 Electrical Characterization

Step-1: Capacitance of different layers of sensing platform and at antigen-antibody conjugation: The capacitance is measured at various stages consisting of different sub-layers. All the measurement s were taken using two point probe station and the dielectric parameters were calculated by using Agilent 4284A Precision LCR meter. The frequency range was taken from 10 kHz-100 kHz for all the sub-layers with a succession of 10 kHz at each interval.

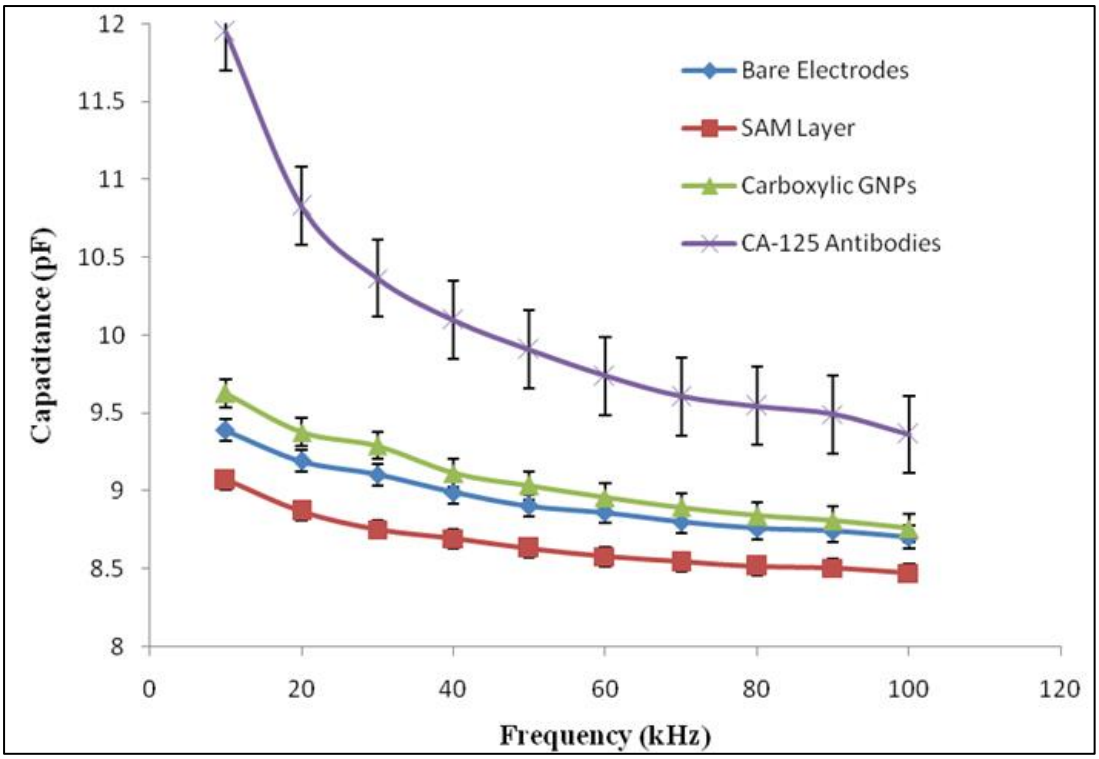

Figure 4.5 Capacitance vs. frequency plot for different layers on top of sensor.

The Figure 4.5 shows the plot of capacitance vs. frequency at different sub-layers. The highest capacitance of the bare interdigitated electrodes was recorded 9.38 pF at 10 kHz and the least 8.70 pF at 100 kHz. The capacitance values of the SAM layer (Thiourea) having higher electron transfer resistance was found to

be lower than bare electrodes. The highest values were recorded 9.06 pF at 10 kHz and the least 8.47 pF at 100 kHz. The LCR meter measures the impedance of the net circuit and converts into the equivalent capacitance based on the real and imaginary parts of the impedance. The capacitance of the SAM layer is observed to be lower than that of the bare electrodes. The potential reason is the higher charge transfer resistance of the SAM layer which directly affects the real part of the impedance. This increment in the resistance directly influences and increases the net impedance. As a result of this phenomena, the net capacitance of the circuit decreases over frequency [49].

The gold nanoparticles (GNPs) exhibiting excellent electrical, chemical and structural properties make it highly promising for nanoscale sensing. The gold nanoparticles having higher permittivity resulted in slightly higher capacitance to that of both bare electrodes and the SAM layer which is around 9.62 pF at 10 kHz and 8.76 pF at 100 kHz.

The experiment used the antigens solution which consists of CA-125 antigens in Phosphate Buffer Saline (PBS) solvent. In the first half of the experiment, bare PBS solution without the CA-125 antigens was used for sensing to refer it as a baseline. A drop of PBS solution (approximately 5µl) was placed at the inlet of the microchannel of the biosensor. The PBS solution passed through the microchannel due to the capillary effect and the dielectric measurements were taken in the frequency range from 10-100 kHz. The capacitance values almost remained

unchanged over the same frequency range. The capacitance curve of the bare PBS solution was regarded as the 'Baseline'. The highest and lowest capacitive values of the 'Baseline' curve were measured to be 99.74 pF and 93.04 pF respectively.

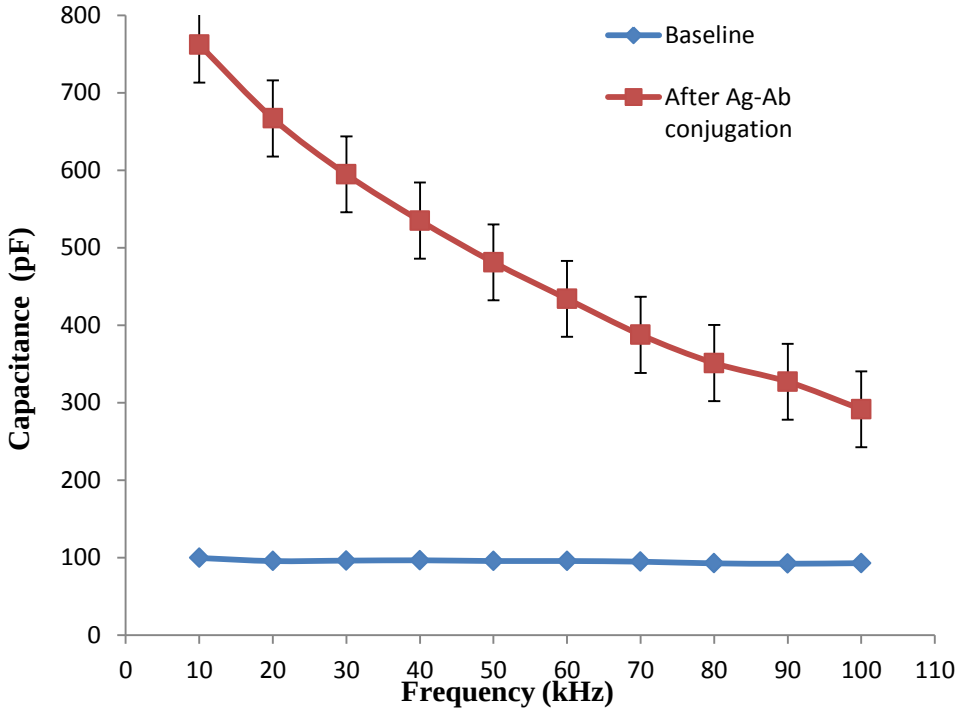

Figure 4.6 Capacitance vs. frequency plot for the Baseline and after Ag-Ab conjugation

The antigens and the antibodies interaction are very selective and specific. The specific antigens and antibodies interactions form a complex which increases the net molecular size. The change in the size of the complex disturbs or interfere the distribution of the charges present in the dielectric medium. The antigens – antibodies complex creates an effect in the distribution of charges within the dielectric region which results in dipole moment. As a result of this phenomenon, the polarization is created due to the dipole-dipole interaction within the dielectric interface [48-51]. Thus, the dielectric values of each antigen-antibody complex over the range of frequencies have its unique variation which is intended to analyze and

check for the significant changes. The measured impedance or capacitance of the biosensor varies with the relative changes in dielectric properties on sensor surface. The Figure 4.6 shows the plot between the capacitance and frequency of the 'Baseline' and 'after the antigen- antibody conjugation'.

The antigens solution flows through the microfluidic channel and the interaction between the antigens and the antibodies takes place which results in the change of dielectric properties of the medium over the sensor surface. The change in the dielectric properties directly influences the change in the capacitance over a range of frequency. The highest capacitance values are observed at 10 kHz for both 'Baseline' and after the Ag-Ab conjugation in the selected frequency range. The capacitance of the 'Baseline' is around 12 pF and is increased to a value around 689 pF after the antigens interaction. The significant change in the capacitance values represents the conjugation of the CA-125 antigens and antibodies. The plot also demonstrates the functionality of the gold nanoparticles based interdigitated electrodes biosensor.

Step-2: Capacitance measurement comparison of CA-125 antigen-antibody conjugation at static and microfluidic flow condition: The plot in Figure 4.7 specifies about the stability of the gold nanoparticles under shear flow conditions. The carboxylic gold nanoparticles sensing platform without the microchannel (static condition) resulted in consistently higher capacitance variation due antigens and antibodies interaction. The highest capacitance is recorded to be 762.13 pF at 10

kHz and the least 291.71 pF at 100 kHz. Due to the lack of any shear flow condition, the stability of the gold nanoparticles and the biomarkers is significantly higher which enhanced the sensitivity. Another set of experiment is performed with the PDMS microfluidic channel microchannel with the width of 'W' (300um) and depth of 'h' (107um) on the sensing platform with gold nanoparticles. Both the experiments have exactly the same sensing composition but the second set of the experiment was performed with microchannel to check the sensitivity of the biosensor. The antigens solution flows through the microchannel on top of the biosensor due to the capillary effect of the antigen solution. When the antigen solution flow through the microchannel the shear caused by the flow on the sensing platform makes the sensing surface unstable.

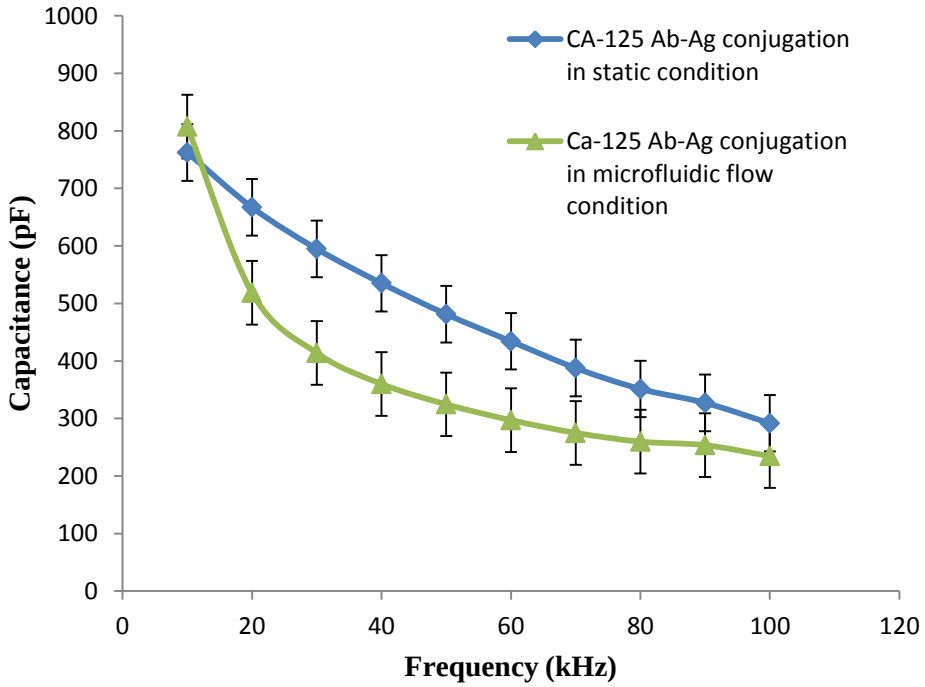

Figure 4.7 Capacitance vs. frequency plot for different gold nanoparticles under static and dynamic conditions.

The capacitance was recorded from highest 807.30 pF to lowest 234.51 pF

within the frequency range from 10-100 kHz during the flow of antigen solution in the microchannel. The tight confinement of the fluid flow layer in the microchannel exerts high surface shear stress which can impact the stabilization of the antibodies that are binded to the sensing platform [25 & 26]. The shear force applied by the fluid on the surface of the sensing platform in microchannel induces mechanical breakage of the weak bonds of the antibodies with the sensing platform [27-29]. The breakage in bonds results in the increase in instability of the immobilized antibodies. So due to lack of any shear in 'static' condition, the stability of the CA-125 antibody was significantly higher which directly enhanced the sensitivity.

4.3 Conclusions

In the current study, the sensitivity variation due to microfluidic flow was established by detecting the CA-125 antigens from biofluid using gold interdigitated electrodes. Based on the measured results, the following conclusions can be made: (1) The functionality of the individual layers in the sensing platform is validated with the changes in the capacitance measurements. (2) The detection of the CA-125 antigens using the gold nano particles on interdigitated electrodes in the microfluidic flow condition is verified by the change in the capacitance signal with the PBS solution and the antigen solution. (3) The capacitive sensitivity of the antigen-antibody interaction is lower with 'microfluidic flow' condition than 'static' condition. The carboxylic gold nanoparticles based interdigitated electrodes biosensor can be modified further based on the antigens and antibodies

configuration serve as a promising platform for lowering the detection limit even under dynamic conditions.

CHAPTER 5

RESEARCH SUMMARY

5.1 Summary

The research study performed on the capacitive sensing during the detection of the CA-125 antigen at different condition of the antibody immobilization using the chemical treatment (Thiourea and Glutaraldehyde) and nano particles (carboxylic gold nano particles). In this research, the CA-125 antigens are successfully detected with the microfluidic biosensor with the difference in the capacitive signal response before and after the antigen-antibody conjugation. Also the study was performed to understand the capacitive signal response under microfluidic flow condition and static condition on the sensing platform. This study of capacitive variation due to microfluidic flow helps to have detailed understanding of the bioconjugation and immobilization of the targeted probes in the microfluidic biosensors. Due to the high orientational freedom for the antibodies to immobilize on the gold nano particles, there was a high capacitive signal response when compared to the antibodies immobuilized with the chemical treatment. Though the immobilization of the antibodies on the sensing platform has shown better sensitivity with high signal response, the effect of the microfluidic flow still yielded to lower signal response when compared to the static drop condition. As the major challenge in the microfluidic biosensor assays is washing steps which required creative engineering steps this study helps to researchers to develop the novel immobilization techniques

for enhanced sensitivity of the immuno microfluidic biosensors.

5.2 Future Research Scope

The future scope of this research will be detection of the multiple antigens from the single biofluid sample, with individual signal responses from individual sensing platform under the microchannel of the biosensor. The signal responses from the different targeted probes (antibodies) from each sensing platform will provide the information of the existence of the different antigens in the biofluid sample. Detection of multiple antigens from the single biofluid helps in enhanced specificity of the biosensor. Also, the future scope includes the detection of the antigens with multiple concentrations in the biofluid sample. The detection of the multiple antigens with multiple concentrations provide enhanced sensing mechanism which is highly specific and highly sensitive.

REFERENCES

[1] Buerk, D. G. (2004). Measuring tissue PO2 with microelectrodes. In Methods in enzymology (Vol. 381, pp. 665-690). Academic Press.

[2] Perumal, V., & Hashim, U. (2014). Advances in biosensors: Principle, architecture and applications. Journal of Applied Biomedicine, 12(1), 1-15.

[3] Kirsch, J., Siltanen, C., Zhou, Q., Revzin, A., & Simonian, A. (2013). Biosensor technology: recent advances in threat agent detection and medicine. Chemical Society Reviews, 42(22), 8733-8768.

[4] Vadgama, P., & Crump, P. W. (1992). Biosensors: recent trends. A review. Analyst, 117(11), 1657-1670.

[5] Grieshaber, D., MacKenzie, R., Voeroes, J., & Reimhult, E. (2008). Electrochemical biosensors-sensor principles and architectures. Sensors, 8(3), 1400-1458.

[6] Ronkainen, N. J., Halsall, H. B., & Heineman, W. R. (2010). Electrochemical biosensors. Chemical Society Reviews, 39(5), 1747-1763.

[7] Daniels, J. S., & Pourmand, N. (2007). Label‐free impedance biosensors: Opportunities and challenges. Electroanalysis, 19(12), 1239-1257.

[8] Berggren, C., Bjarnason, B., & Johansson, G. (2001). Capacitive biosensors. Electroanalysis: An International Journal Devoted to Fundamental and Practical Aspects of Electroanalysis, 13(3), 173-180.

[9] Tsouti, V., Boutopoulos, C., Zergioti, I., & Chatzandroulis, S. (2011). Capacitive microsystems for biological sensing. Biosensors and Bioelectronics, 27(1), 1-11.

[10] Kumar, S., Kumar, S., Ali, M., Anand, P., Agrawal, V. V., John, R., ... & Malhotra, B. D. (2013). Microfluidic‐integrated biosensors: Prospects for point‐of‐care diagnostics. Biotechnology journal, 8(11), 1267-1279.

[11] Itoh, D., Sassa, F., Nishi, T., Kani, Y., Murata, M., & Suzuki, H. (2012). Droplet-based microfluidic sensing system for rapid fish freshness determination. Sensors and Actuators B: chemical, 171, 619-626.

[12] Puigmartí-Luis, Josep. "Microfluidic platforms: a mainstream technology for the preparation of crystals." Chemical Society Reviews 43, no. 7 (2014): 2253-2271.

[13] Puigmartí-Luis, J. (2014). Microfluidic platforms: a mainstream technology for the preparation of crystals. Chemical Society Reviews, 43(7), 2253-2271.

[14] Mark, D., Haeberle, S., Roth, G., Von Stetten, F., & Zengerle, R. (2010). Microfluidic lab-on-a-chip platforms: requirements, characteristics and applications. In Microfluidics Based Microsystems (pp. 305-376). Springer, Dordrecht.

[15] Ma, X., Wu, Y., Jin, S., Tian, Y., Zhang, X., Zhao, Y., ... & Liang, X. J. (2011). Gold nanoparticles induce autophagosome accumulation through size-dependent nanoparticle uptake and lysosome impairment. ACS nano, 5(11), 8629-8639.

[16] Tiwari, P. M., Vig, K., Dennis, V. A., & Singh, S. R. (2011). Functionalized gold nanoparticles and their biomedical applications. Nanomaterials, 1(1), 31-63.

[17] Jazayeri, M. H., Amani, H., Pourfatollah, A. A., Pazoki-Toroudi, H., & Sedighimoghaddam, B. (2016). Various methods of gold nanoparticles (GNPs) conjugation to antibodies. Sensing and bio-sensing research, 9, 17-22.

[18] Loyprasert, S., Thavarungkul, P., Asawatreratanakul, P., Wongkittisuksa, B., Limsakul, C., & Kanatharana, P. (2008). Label-free capacitive immunosensor for microcystin-LR using self-assembled thiourea monolayer incorporated with Ag nanoparticles on gold electrode. Biosensors and Bioelectronics, 24(1), 78-86.

[19] Sperling, R. A., & Parak, W. J. (2010). Surface modification, functionalization and bioconjugation of colloidal inorganic nanoparticles. Philosophical Transactions of the Royal Society of London A: Mathematical, Physical and Engineering Sciences, 368(1915), 1333-1383.

[20] "What Is CA-125 - Ovarian Cancer Research Fund Alliance". 2017. Ovarian Cancer Research Fund Alliance. https://ocrfa.org/patients/about-ovarian-cancer/symptoms-and-detection/what-is-ca-125/.

[21] Quest Diagnostics Incorporated, 2017. CA-125(Test code: 29256 & CPT Code(s)86304. http://www.questdiagnostics.com/testcenter/BUOrderInfo.action?tc=29256&labCode=PHP

[22] American Cancer Society. Cancer Facts & Figures 2017. Atlanta; American Cancer Society; 2017

[23] Goddard, J. M., & Erickson, D. (2009). Bioconjugation techniques for microfluidic biosensors. Analytical and bioanalytical chemistry, 394(2), 469.

[24] Ichikawa, N., Hosokawa, K., & Maeda, R. (2004). Interface motion of capillary-driven flow in rectangular microchannel. Journal of colloid and interface science, 280(1), 155-164.

[25] Ginn, B. T., & Steinbock, O. (2003). Polymer surface modification using microwave-oven-generated plasma. Langmuir, 19(19), 8117-8118.

[26] Xiao, D., Zhang, H., & Wirth, M. (2002). Chemical modification of the surface of poly (dimethylsiloxane) by atom-transfer radical polymerization of acrylamide. Langmuir, 18(25), 9971-9976.

[27] Eddington, D. T., Puccinelli, J. P., & Beebe, D. J. (2006). Thermal aging and reduced hydrophobic recovery of polydimethylsiloxane. Sensors and Actuators B: Chemical, 114(1), 170-172.

[28] Tan, S. H., Nguyen, N. T., Chua, Y. C., & Kang, T. G. (2010). Oxygen plasma treatment for reducing hydrophobicity of a sealed polydimethylsiloxane microchannel. Biomicrofluidics, 4(3), 032204.

[29] Tsouti, V., Boutopoulos, C., Zergioti, I., & Chatzandroulis, S. (2011). Capacitive microsystems for biological sensing. Biosensors and Bioelectronics, 27(1), 1-11.

[30] Zhu, X., & Ahn, C. H. (2005). Electrochemical determination of reversible redox species at interdigitated array micro/nanoelectrodes using charge injection method. IEEE transactions on nanobioscience, 4(2), 164-169.

[31] Zou, Z., Kai, J., Rust, M. J., Han, J., & Ahn, C. H. (2007). Functionalized nano interdigitated electrodes arrays on polymer with integrated microfluidics for direct bio-affinity sensing using impedimetric measurement. Sensors and Actuators A: Physical, 136(2), 518-526.

[32] Loyprasert, S., Thavarungkul, P., Asawatreratanakul, P., Wongkittisuksa, B., Limsakul, C., & Kanatharana, P. (2008). Label-free capacitive immunosensor for microcystin-LR using self-assembled thiourea monolayer incorporated with Ag nanoparticles on gold electrode. Biosensors and Bioelectronics, 24(1), 78-86.

[33] Sperling, R. A., & Parak, W. J. (2010). Surface modification, functionalization and bioconjugation of colloidal inorganic nanoparticles. Philosophical Transactions of the Royal Society of London A: Mathematical, Physical and Engineering Sciences, 368(1915), 1333-1383.

[34] Altintas, Z., Kallempudi, S. S., & Gurbuz, Y. (2014). Gold nanoparticle modified capacitive sensor platform for multiple marker detection. Talanta, 118, 270-276.

[35] Li, X., Yu, M., Chen, Z., Lin, X., & Wu, Q. (2017). A sensor for detection of carcinoembryonic antigen based on the polyaniline-Au nanoparticles and gap-based interdigitated electrode. Sensors and Actuators B: Chemical, 239, 874-882.

[36] Pingarrón, J. M., Yanez-Sedeno, P., & González-Cortés, A. (2008). Gold nanoparticle-based electrochemical biosensors. Electrochimica Acta, 53(19), 5848-5866.

[37] Raghav, R., & Srivastava, S. (2015). Core–shell gold–silver nanoparticles based impedimetric immunosensor for cancer antigen CA125. Sensors and Actuators B: Chemical, 220, 557-564.

[38] Nunna, B. B., Mandal, D., Zhuang, S., & Lee, E. S. (2017). Innovative Point-of-Care (POC) Micro Biochip for Early Stage Ovarian Cancer Diagnostics. Sensors & Transducers, 214(7).

[39] Kallempudi, S. S., & Gurbuz, Y. (2011). A nanostructured-nickel based interdigitated capacitive transducer for biosensor applications. Sensors and Actuators B: Chemical, 160(1), 891-898.

[40] Mandal, D., Nunna, B. B., Zhuang, S., Rakshit, S., & Lee, E. S. (2017). Carbon nanotubes based biosensor for detection of cancer antigens (CA-125) under shear flow condition. Nano-Structures & Nano-Objects.

[41] Li, X., Yu, M., Chen, Z., Lin, X., & Wu, Q. (2017). A sensor for detection of carcinoembryonic antigen based on the polyaniline-Au nanoparticles and gap-based interdigitated electrode. Sensors and Actuators B: Chemical, 239, 874-882.

[42] A Abdulbari, H., & A Basheer, E. (2017). Investigating the Enhancement of Microfluidics-Based Electrochemical Biosensor Response with Different Microchannel Dimensions. Current Analytical Chemistry, 13(5), 361-369.

[43] Quail, M. A. (2010). DNA: Mechanical breakage. eLS.

[44] Altintas, Z., Kallempudi, S. S., & Gurbuz, Y. (2014). Gold nanoparticle modified capacitive sensor platform for multiple marker detection. Talanta, 118, 270-276.

[45] Li, X., Yu, M., Chen, Z., Lin, X., & Wu, Q. (2017). A sensor for detection of carcinoembryonic antigen based on the polyaniline-Au nanoparticles and gap-based interdigitated electrode. Sensors and Actuators B: Chemical, 239, 874-882.

[46] Pingarrón, J. M., Yanez-Sedeno, P., & González-Cortés, A. (2008). Gold nanoparticle-based electrochemical biosensors. Electrochimica Acta, 53(19), 5848-5866.

[47] Raghav, R., & Srivastava, S. (2015). Core–shell gold–silver nanoparticles based impedimetric immunosensor for cancer antigen CA125. Sensors and Actuators B: Chemical, 220, 557-564.

[48] Limbut, W., Kanatharana, P., Mattiasson, B., Asawatreratanakul, P., & Thavarungkul, P. (2006). A reusable capacitive immunosensor for carcinoembryonic antigen (CEA) detection using thiourea modified gold electrode. Analytica chimica acta, 561(1-2), 55-61.

[49] Kallempudi, S. S., & Gurbuz, Y. (2011). A nanostructured-nickel based interdigitated capacitive transducer for biosensor applications. Sensors and Actuators B: Chemical, 160(1), 891-898.

[50] Mandal, D., Nunna, B. B., Zhuang, S., Rakshit, S., & Lee, E. S. (2017). Carbon nanotubes based biosensor for detection of cancer antigens (CA-125) under shear flow condition. Nano-Structures & Nano-Objects.

[51] Nunna, B. B., Mandal, D., Zhuang, S., & Lee, E. S. (2017). Innovative Point-of-Care (POC) Micro Biochip for Early Stage Ovarian Cancer Diagnostics. Sensors & Transducers, 214(7).

[52] Tiwari, P. M., Vig, K., Dennis, V. A., & Singh, S. R. (2011). Functionalized gold nanoparticles and their biomedical applications. Nanomaterials, 1(1), 31-63.

[53] Jazayeri, M. H., Amani, H., Pourfatollah, A. A., Pazoki-Toroudi, H., & Sedighimoghaddam, B. (2016). Various methods of gold nanoparticles (GNPs) conjugation to antibodies. Sensing and bio-sensing research, 9, 17-22.

[54] Ghasemi, N., Ghobadzadeh, S., Zahraei, M., Mohammadpour, H., Bahrami, S., & Rajabi, S. (2014). HE4 combined with CA125: favorable screening tool for ovarian cancer. Medical Oncology, 31(1), 808.

[55] Le, M. H., Jimenez, C., Chainet, E., & Stambouli, V. (2015). A label-free impedimetric DNA sensor based on a nanoporous SnO2 film: Fabrication and detection performance. Sensors, 15(5), 10686-10704.

[56] Sato, K., Takahashi, S., & Anzai, J. I. (2012). Layer-by-layer thin films and microcapsules for biosensors and controlled release. Analytical Sciences, 28(10), 929-938.

[57] Khalil, I., Julkapli, N. M., Yehye, W. A., Basirun, W. J., & Bhargava, S. K. (2016). Graphene–Gold Nanoparticles Hybrid—Synthesis, Functionalization, and Application in a Electrochemical and Surface-Enhanced Raman Scattering Biosensor. Materials, 9(6), 406.

[58] Lazcka, O., Del Campo, F. J., & Munoz, F. X. (2007). Pathogen detection: A perspective of traditional methods and biosensors. Biosensors and bioelectronics, 22(7), 1205-1217.

[59] Tsouti, V., Boutopoulos, C., Zergioti, I., & Chatzandroulis, S. (2011). Capacitive microsystems for biological sensing. Biosensors and Bioelectronics, 27(1), 1-11.

[60] Perumal, V., & Hashim, U. (2014). Advances in biosensors: Principle, architecture and applications. Journal of Applied Biomedicine, 12(1), 1-15.

[61] Laczka, O., Baldrich, E., Muñoz, F. X., & del Campo, F. J. (2008). Detection of Escherichia coli and Salmonella typhimurium using interdigitated microelectrode capacitive immunosensors: the importance of transducer geometry. Analytical chemistry, 80(19), 7239-7247.

[62] Berggren, C., Bjarnason, B., & Johansson, G. (2001). Capacitive biosensors. Electroanalysis: An International Journal Devoted to Fundamental and Practical Aspects of Electroanalysis, 13(3), 173-180.

[63] Macdonald, J. R. (1987). Impedance spectroscopy and its use in analyzing the steady-state AC response of solid and liquid electrolytes. Journal of electroanalytical chemistry and interfacial electrochemistry, 223(1-2), 25-50.

[64] Zhu, X., & Ahn, C. H. (2005). Electrochemical determination of reversible redox species at interdigitated array micro/nanoelectrodes using charge injection method. IEEE transactions on nanobioscience, 4(2), 164-169.

[65] Ayliffe, H. E., Frazier, A. B., & Rabbitt, R. D. (1999). Electric impedance spectroscopy using microchannels with integrated metal electrodes. Journal of Microelectromechanical systems, 8(1), 50-57.

[66] Mamishev, A. V., Sundara-Rajan, K., Yang, F., Du, Y., & Zahn, M. (2004). Interdigital sensors and transducers. Proceedings of the IEEE, 92(5), 808-845.

[67] Gabriel, C., Gabriel, S., & Corthout, E. (1996). The dielectric properties of biological tissues: I. Literature survey. Physics in Medicine & Biology, 41(11), 2231.

[68] Altintas, Z., Kallempudi, S. S., & Gurbuz, Y. (2014). Gold nanoparticle modified capacitive sensor platform for multiple marker detection. Talanta, 118, 270-276.

[69] Altintas, Z., Kallempudi, S. S., Sezerman, U., & Gurbuz, Y. (2012). A novel magnetic particle-modified electrochemical sensor for immunosensor applications. Sensors and Actuators B: Chemical, 174, 187-194.

[70] Jacobs, C. B., Peairs, M. J., & Venton, B. J. (2010). Carbon nanotube based electrochemical sensors for biomolecules. Analytica chimica acta, 662(2), 105-127.

[71] Ma, X., Wu, Y., Jin, S., Tian, Y., Zhang, X., Zhao, Y., ... & Liang, X. J. (2011). Gold nanoparticles induce autophagosome accumulation through size-dependent nanoparticle uptake and lysosome impairment. ACS nano, 5(11), 8629-8639.

[72] Loyprasert, S., Thavarungkul, P., Asawatreratanakul, P., Wongkittisuksa, B., Limsakul, C., & Kanatharana, P. (2008). Label-free capacitive immunosensor for microcystin-LR using self-assembled thiourea monolayer incorporated with Ag nanoparticles on gold electrode. Biosensors and Bioelectronics, 24(1), 78-86.

[73] Sperling, R. A., & Parak, W. J. (2010). Surface modification, functionalization and bioconjugation of colloidal inorganic nanoparticles. Philosophical Transactions of the Royal Society of London A: Mathematical, Physical and Engineering Sciences, 368(1915), 1333-1383.

[74] Altintas, Z., Kallempudi, S. S., & Gurbuz, Y. (2014). Gold nanoparticle modified capacitive sensor platform for multiple marker detection. Talanta, 118, 270-276.

[75] Li, X., Yu, M., Chen, Z., Lin, X., & Wu, Q. (2017). A sensor for detection of carcinoembryonic antigen based on the polyaniline-Au nanoparticles and gap-based interdigitated electrode. Sensors and Actuators B: Chemical, 239, 874-882.

[76] Pingarrón, J. M., Yanez-Sedeno, P., & González-Cortés, A. (2008). Gold nanoparticle-based electrochemical biosensors. Electrochimica Acta, 53(19), 5848-5866.

[77] Huang, C., & Tsou, C. (2014). The implementation of a thermal bubble actuated microfluidic chip with microvalve, micropump and micromixer. Sensors and Actuators A: Physical, 210, 147-156.

[78] Erickson, D., Liu, X., Venditti, R., Li, D., & Krull, U. J. (2005). Electrokinetically based approach for single-nucleotide polymorphism discrimination using a microfluidic device. Analytical chemistry, 77(13), 4000-4007.

[79] Daniels, J. S., & Pourmand, N. (2007). Label‐free impedance biosensors: Opportunities and challenges. Electroanalysis, 19(12), 1239-1257.

[80] Berggren, Christine, and Gillis Johansson. "Capacitance measurements of antibody− antigen interactions in a flow system." Analytical Chemistry 69, no. 18 (1997): 3651-3657.